HHS Public Access

Author manuscript

Cell Rep. Author manuscript; available in PMC 2019 December 16.

Published in final edited form as:

Cell Rep. 2019 November 26; 29(9): 2849–2861.e6. doi:10.1016/j.celrep.2019.10.081.

Developmental Rewiring between Cerebellar Climbing Fibers and Purkinje Cells Begins with Positive Feedback Synapse Addition

Alyssa Michelle Wilson[1,7,*], **Richard Schalek**[2], **Adi Suissa-Peleg**[2,3], **Thouis R. Jones**[4], **Seymour Knowles-Barley**[5], **Hanspeter Pfister**[3], **Jeff William Lichtman**[6,*]

[1]Princeton Neuroscience Institute, Princeton University, Princeton, NJ 08540, USA [2]Center for Brain Science, Harvard University, Cambridge, MA 02138, USA [3]School of Engineering and Applied Sciences, Harvard University, Cambridge, MA 02138, USA [4]Broad Institute, Cambridge, MA 02142, USA [5]Volpara Health Technologies, Wellington 6011, New Zealand [6]Department of Molecular and Cellular Biology, Harvard University, Cambridge, MA 02138, USA [7]Lead Contact

SUMMARY

During postnatal development, cerebellar climbing fibers alter their innervation strengths onto supernumerary Purkinje cell targets, generating a one-to-few connectivity pattern in adulthood. To get insight about the processes responsible for this remapping, we reconstructed serial electron microscopy datasets from mice during the first postnatal week. Between days 3 and 7, individual climbing fibers selectively add many synapses onto a subset of Purkinje targets in a positive-feedback manner, without pruning synapses from other targets. Active zone sizes of synapses associated with powerful versus weak inputs are indistinguishable. Changes in synapse number are thus the predominant form of early developmental plasticity. Finally, the numbers of climbing fibers and Purkinje cells in a local region nearly match. Initial over-innervation of Purkinje cells by climbing fibers is therefore economical: the number of axons entering a region is enough to assure that each ultimately retains a postsynaptic target and that none branched there in vain.

In Brief

Wilson et al. use electron microscopy to reveal that developmental rewiring in the cerebellum begins with significant synapse addition by climbing fibers onto a few preferred Purkinje cells. They also find that rewiring is economical: all climbing fibers initially entering a cerebellar region play a role in final connectivity there.

*Correspondence: amw7@princeton.edu (A.M.W.), jeff@mcb.harvard.edu (J.W.L.).

AUTHOR CONTRIBUTIONS

Conceptualization, A.M.W. and J.W.L.; Methodology, A.M.W. and J.W.L.; Software, A.M.W., A.S.-P., T.R.J., S.K.-B., and H.P.; Formal Analysis, A.M.W. and J.W.L.; Investigation, A.M.W.; Resources, J.W.L. and R.S.; Data Curation, A.M.W., A.S.-P., T.R.J., S.K.-B., and H.P.; Writing – Original Draft, A.M.W. and J.W.L.; Writing – Review & Editing, A.M.W. and J.W.L.; Visualization, A.M.W. and J.W.L.; Supervision, J.W.L.; Funding Acquisition, A.M.W. and J.W.L.

DECLARATION OF INTERESTS

R.S. and J.W.L. are inventors on US Patent 10288532 for the ATUM used in this work.

SUPPLEMENTAL INFORMATION

Supplemental Information can be found online at https://doi.org/10.1016/j.celrep.2019.10.081.

Graphical Abstract

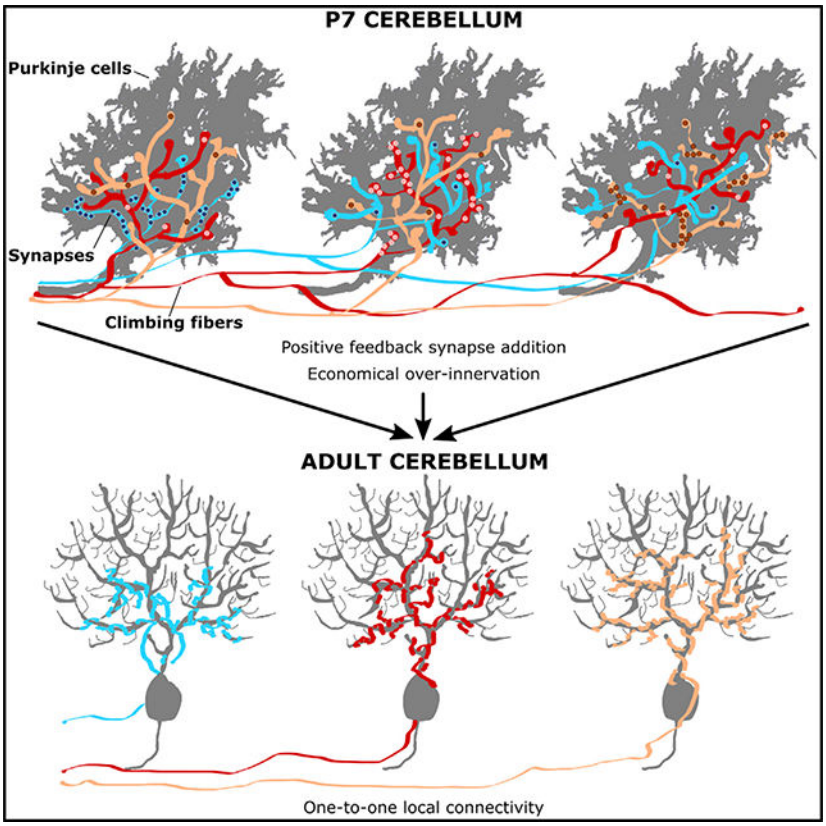

INTRODUCTION

In many vertebrates, neurons undergo extensive rewiring during postnatal development, removing synapses from some of their initial target cells and eventually achieving neural circuitry that is refined from what was initially an overconnected network. This process, known as synapse elimination, occurs in the central nervous system (CNS) and peripheral nervous system (PNS). One of the most striking examples of synapse elimination in the CNS occurs in the cerebellum, where connections between climbing fibers and Purkinje cells are modified. This phenomenon has been studied extensively in rodents, where shortly after birth, multiple climbing fibers innervate Purkinje cells (Crepel et al., 1976; Mariani and Changeux, 1981). By the end of the third postnatal week in rodents, only one climbing fiber innervates each Purkinje cell (Kano et al., 2018; Hashimoto and Kano, 2013). The transition from multiple climbing fiber inputs to one parallels the most well-known example of synapse elimination in the PNS, which occurs between motor axons and muscle fibers at the neuromuscular junction (NMJ). Perinatally, ~10 motor axons innervate each muscle fiber in a muscle (Tapia et al., 2012), but almost immediately after birth axons begin removing synapses from some muscle fibers. Live cell imaging *in vivo* shows that the remaining inputs increase their synaptic territory through takeover of sites occupied by other axons until only one axon innervates each muscle fiber (Walsh and Lichtman, 2003; Turney and Lichtman, 2012). This implies that at the NMJ addition of synaptic territory is causally related to the

vacation of sites occupied by axons being pruned and supports the idea that this reorganization is based on a competition between axons vying to innervate the same postsynaptic cell.

Cerebellar synapse elimination is more challenging to study because the cerebellar cortex is less accessible than the neuromuscular system, so that live imaging is difficult (Carrillo et al., 2013). In addition, climbing fibers and Purkinje cell geometries change considerably during early postnatal life as connectivity is being refined (Chedotal and Sotelo, 1993; Ramón y Cajal, 1995).

From an electrophysiological perspective, it is clear that there are several stages of climbing fiber-Purkinje cell synaptic refinement during development. Around postnatal day 3 (P3), climbing fiber-Purkinje cell synapses become detectable in electrophysiological recordings (Mariani and Changeux, 1981). Several studies have estimated the number of climbing fibers innervating a Purkinje cell to be typically 5 or fewer at this age, with all producing similar postsynaptic responses (Bosman et al., 2008; Mariani and Changeux, 1981; Scelfo and Strata, 2005). There is controversy over when this situation changes. Some work suggests that during the first postnatal week, one recorded climbing fiber input to a Purkinje cell becomes more powerful than the others (Hashimoto and Kano, 2003; Bosman et al., 2008). However, other researchers have found that this change does not occur until the second postnatal week (Scelfo and Strata, 2005), coincident with the initial loss of climbing fiber input. By the third week, virtually every Purkinje cell is innervated by one climbing fiber. The elimination process from P7 to beyond P10 has also been subdivided into three stages. Between P7 and P9, some electrophysiologically weak climbing fiber inputs disappear. At P9 to P10, the rise times associated with quanta of one of the remaining climbing fibers become longer (Hashimoto et al., 2009). Anatomical studies show that this phenomenon occurs as one climbing fiber begins its “climb” up the newly formed apical dendrite (Carrillo et al., 2013). After P10, the few remaining climbing fibers that did not grow onto the apical dendrite progressively are lost and no longer elicit postsynaptic responses.

In this study, we aimed to resolve an important question about developmental rewiring of climbing fibers: are synapse strengthening and removal concurrent or sequential? Previous work has identified climbing fiber functional differentiation but cannot distinguish whether that differentiation is a result of synaptic strengthening only or strengthening coupled with synapse removal. This is an important question because the answer provides insight into the underlying mechanism of developmental reorganization. For example, if synapse addition and elimination are occurring at the same time then, as at the NMJ, addition may be the consequence of loss, thus climbing fiber rearrangement could be a takeover-based competition. If, however, synapse addition is independent of synapse elimination, then the competitive mechanism described above for NMJ synapse elimination might be inadequate to explain the way this CNS reorganization takes place.

We also wanted to answer more specific questions about how changes in relative climbing fiber innervation strength are manifested. First, do climbing fibers alter their innervation strengths by adding and removing synapses, by growing or shrinking individual synapses, or by a combination of these two phenomena? We are interested in this question because one

limitation of the NMJ as a model of events in the CNS is that the NMJ looks different than typical CNS synapses. In the NMJ, takeover-based growth leads to synapses that are large contiguous structures with many presynaptic release sites and quantal contents of ~100 (Slater, 2017). By contrast, CNS synapses are often single synaptic boutons with one or several release sites and quantal contents of ~1 (although some are substantially larger, e.g., calyx synapses with quantal contents of >300; Iwasaki and Takahashi, 2001). Thus, climbing fiber synaptic strengthening could occur either by enlarging each synapse to have more release sites (by a small or large amount) or by adding more boutons.

Furthermore, how does relative strengthening of climbing fiber synapses progress during early postnatal development? Finally, how do immature climbing fibers parse out their synapses among many different Purkinje cells in a local region of cerebellar cortex?

To explore these questions, we analyzed the connectivity of climbing fibers to Purkinje cells at P3 and P7 using serial-section scanning electron microscopy. We chose these time points because some evidence suggests that this stage is when functional changes begin (Kano et al., 2018). Our results show that climbing fibers dramatically change their connectivity during this time by preferentially adding synapses onto some target cells. These results indicate that climbing fiber-Purkinje cell synaptic reorganization begins with axons choosing to establish additional synapses onto a small number of preferred partners among the cohort of Purkinje cells they innervate. In addition, we see no sign of any synapse loss. The connectivity we observe is well explained by a rich-get-richer process of synapse addition, also known as preferential attachment, by climbing fibers onto their preferred targets. Finally, the connectomics approach allowed us to learn about the population of climbing fibers that initially over-innervate the Purkinje cells in a region of cerebellar cortex. We find that the numbers of climbing fibers and Purkinje cells about match locally (as in adulthood), implying that all climbing fibers branching in an area are able to play a role in the final connectivity pattern.

RESULTS

The Datasets

These cerebellar datasets came from two developing mice, one at P3 and one at P7. Because we wished to compare them, for each we prepared a block from the medial cerebellar vermis and imaged the anterior root of lobule VIII (Figures 1A, 1B, and 1G). We used the same region at each time because the climbing fiber developmental timeline is delayed for some lobules relative to others, and within each lobule timelines also shift with position (outer regions often develop earlier than inner regions; Armengol and Sotelo, 1991; Ramón y Cajal, 1995). For both blocks, we imaged a column of tissue from the pia to the white matter in order to capture Purkinje cell dendrites and axons to the fullest extent possible. Purkinje cells are the only cerebellar cells that consistently send their axons into the white matter, so this was an easy way to identify them. At the root of the lobule, we also collected tissue closer to proximal branch points of climbing fibers, which helped us reconstruct them more fully. Each block was cut into 30-nm thick sections in the sagittal plane (STAR Methods). A total of 1,658 sections for the P3 block and 2,514 sections for the P7 block were imaged at 4-nm/px resolution in a scanning electron microscope. In both datasets the imaged region

measured 190 μm radially × 120 μm tangentially. The acquired image volume was 1.1×10^6 μm^3 at P3 and 1.7×10^6 μm^3 at P7 (Figure 1C).

Cytoarchitecture of the Cerebellum at Two Developmental Ages

All cortical layers were visible in both datasets. The thicknesses of some layers differed between the two ages, as expected (Figure S1A). The external granular layer and molecular layer were substantially thicker at P7 than at P3, consistent with granule cell migration (Sotelo, 2004). Additionally, the Purkinje cell layer was 2 to 3 cells deep at P3 and became a monolayer at P7 (Figures S1B and S1C). The area density of Purkinje cells in the Purkinje cell layer also decreased from P3 to P7 (0.008 cells/μm^2 at P3, 0.003 cells/μm^2 at P7, possibly due to tissue growth). We also observed substantial changes in Purkinje cell geometry (below).

Changing Connectivity Patterns on Cerebellar Purkinje Cells between P3 and P7

In order to reveal how Purkinje cell innervation changed during the first postnatal week, we sampled climbing fiber-Purkinje cell connectivity in both volumes. We began this sampling by reconstructing all synaptic input to one Purkinje cell at each age (STAR Methods; Figure 1D). This task was challenging because dendritic arbors of the immature Purkinje cells were quite complex. At P3 (Figure S1D), dendrites ran in many different directions (in dramatic contrast to the monoplanar geometry of adult Purkinje dendrites) and made frequent side branches. The arbor thus ramified over a large portion of the image volume, and identifying synapses onto Purkinje cells required scrutiny of nearly the entire volume. We found a total of 464 synapses targeting the P3 cell. At P7 (Figure S1E), although the Purkinje cell had about 3 times fewer dendrites, the dendrites and soma produced a large number of spine-like processes (Sotelo, 2004), many of which were innervated. (Interestingly, a number of these processes ran parallel with nearby parallel fibers—data not shown.) Finding synapses on the P7 cell thus involved tracing out thousands of processes. In total we found 1,124 synapses on the P7 cell.

To identify the climbing fiber inputs to these Purkinje cells, we classified the presynaptic partner for every synapse based on the input axon's morphology and its synaptic connections to other target cells. We found that 352 axon branches formed all the synapses onto the fully reconstructed Purkinje cell in the P3 dataset, and 698 axon branches formed the synapses onto the fully reconstructed Purkinje cell at P7 (Table S1). At both ages it was possible to divide axons into three categories: inhibitory cell axons, granule cell axons (either the initial radial portion or parallel fibers), and non-granule-cell excitatory axons. Nongranule-cell excitatory axons may be either climbing fibers or mossy fibers. We wanted to distinguish between mossy and climbing fiber input, because the main reorganization concerns selection of one climbing fiber input and elimination of the rest, whereas the mossy input is minor during development and then disappears entirely (Mason and Gregory, 1984; Kalinovsky et al., 2011). During the first postnatal week, it was difficult to distinguish these two axon types based on morphology (although they become distinguishable a few days later; Mason and Gregory, 1984). We thus attempted to separate them by their synaptic connectivity. We analyzed the full synaptic connectivity of the excitatory non-granule axon branches and found that they formed two groups, ones forming a majority of their synapses

onto Purkinje cells and ones forming a majority of their synapses onto granule cells. To determine whether the second group was mossy fibers, which target mainly granule cells, we compared the connectivity of the Purkinje cell-innervating axons with that of a separate sample of putative mossy fibers (STAR Methods). We found by several clustering methods (Figure S2; Tables S2 and S3) that these two groups of non-granule excitatory axon branches could be identified as those resembling mossy fibers and those resembling climbing fibers. Through this analysis we identified 55 climbing fiber branches from the 84 non-granule excitatory inputs to the fully reconstructed Purkinje cell at P3 and 49 climbing fiber branches from the 68 non-granule excitatory inputs to the Purkinje cell at P7 (Figures 1E and 1F).

We examined the synaptic connections of all climbing fiber branches innervating the fully reconstructed Purkinje cells at P3 and P7. Despite the fact that a slightly smaller number of climbing fiber branches innervated the P7 Purkinje cell than the P3 cell (49 versus 55, although we show below that these numbers do not represent statistically different numbers of inputs), there was a greater-than-2-fold increase in the total number of synapses formed by those climbing fibers (127 at P3 to 298 at P7). This increase in synapse number was a general feature of individual climbing fiber branches as well (Figures 2A and 2B).

The differing innervation properties we observed for climbing fiber branches at P3 and P7 were confirmed when we expanded our connectivity sample by including all the synapses formed by these axon branches onto other Purkinje cells in the volume (Figures 2C–2F). The 55 climbing fiber branches in the P3 dataset innervated 29 of the 47 other Purkinje cells in the volume (30/48 or 63% of Purkinje cells in total) and allowed analysis of 187 additional climbing fiber-Purkinje cell connections (consisting of 308 additional synapses). The 49 climbing fiber branches at P7 innervated 17 of the 29 other Purkinje cells in the volume (in total 18/30 or 60% of Purkinje cells), contributing 165 additional climbing fiber-Purkinje cell connections and 1,057 synapses. For both ages, the extended data corroborated the analysis above (Figures 2A–2D): climbing fiber branches were establishing greater numbers of synapses at P7 than at P3.

Furthermore, at both ages climbing fiber branches distributed their synapses among Purkinje cells in an inhomogeneous way, in which most climbing fiber-Purkinje cell connections consisted of a few synapses and a small number of connections consisted of many synapses (Figure 2). We considered two different ways that climbing fiber branches could generate the synapse distributions we observed. One possibility is that each climbing fiber branch forms an inhomogeneous distribution of synapses, establishing many synapses with a few Purkinje cell targets and a few synapses with the rest. Alternatively, some climbing fiber branches might establish few synapses with every one of their targets, whereas other climbing fiber branches establish many synapses with each of their targets. To decide between these alternatives, we inspected the number of synapses formed by each climbing fiber branch onto each of its Purkinje targets (Figure 3A; Data S1 and S2). At both P3 and P7 we found that all branches formed only one or two synapses onto most of their Purkinje targets, and at both ages some branches also innervated a few cells with larger numbers of synapses. In neither dataset did we observe a climbing fiber branch that formed only large numbers of synapses onto its Purkinje cell targets. These data argue that developing climbing fibers tend

to act similarly, innervating a large number of Purkinje cells with a few synapses and innervating a few Purkinje cells with many synapses. Furthermore, the large numbers of synapses we observed could not have occurred if climbing fibers distributed synapses among their Purkinje targets with uniform random probability, i.e., without preference (STAR Methods; Figure S3; $p < 0.00001$ for P3 and P7).

This tendency for climbing fibers to distribute a large number of synapses on a small number of cells was more extreme at P7 than P3. At P3, the largest number of synapses we observed a climbing fiber branch to form was 13, but at P7 the largest number of synapses was 45. This difference implies that axons are focusing progressively more synapses on the target cells they prefer.

We next investigated the spatial organization of the uneven distribution of synapses formed by individual climbing fiber branches. In general, branches at P7 formed a higher density of synapses than at P3 (Figure S4A; Wilcoxon rank-sum test, $p = 3 \times 10^{-11}$). At both ages climbing fibers formed synapses onto Purkinje cells somewhat sparsely and at regular intervals as they ramified through the Purkinje cell layer (P3: http://bit.ly/bbandrossP3NGL; P7: http://bit.ly/bbandrossP7NGL; Figure S5A). The one exception to this trend was that some climbing fiber branches with strong Purkinje cell preferences formed higher-density clusters in localized regions (onto the preferred Purkinje cells; Figures S5A–S5D). The Purkinje cells that received large numbers of synapses in these clusters were located at various positions relative to the climbing fiber branch itself. Specifically, preferred cells of a climbing fiber branch did not necessarily overlap maximally with that branch's arbor. In fact, at both ages climbing fiber branches strongly innervated Purkinje cells in a salt and pepper pattern, often making no or very few synapses on an immediate neighbor of a strongly innervated cell (Figures S5E–S5H). These discontinuous innervation patterns suggest that the number of synapses formed by a climbing fiber onto a Purkinje cell is based on a form of selectivity unrelated to Purkinje cell location.

At both P3 and P7, the distributions of synapses established by individual climbing fibers onto Purkinje cells appear to obey a power law. Power laws arise in many systems that undergo growth (Newman, 2005). The power law distribution ($P(k) = Ck^{-\alpha}$, where C and α are constants) determines the proportion of objects $P(k)$ in a system (in this case, synaptically connected climbing fiber-Purkinje cell pairs) that have a particular number k of some quantity (synapses from the climbing fiber branch onto the Purkinje cell). Both synapse distributions were well fit by power law functions (Figures 2C and 2D) with α= 1:75 for P3 and α= 0:96 for P7. These power law distributions could arise from a particular type of growth process known as preferential attachment (Barabási and Albert, 1999). In the climbing fiber-Purkinje cell system, preferential attachment would mean that the tendency of climbing fibers to add synapses increases as the number of synapses they already share with a Purkinje cell target grows larger.

Although there is evidence of massive synaptic pruning in the second postnatal week (measured as a decrease in the number of climbing fiber inputs to a Purkinje cell; Kano et al., 2018), we were interested to learn whether our detailed electron microscopy data showed evidence of climbing fibers removing synapses from Purkinje cells while they added

synapses onto others during the first postnatal week. Because we saw many single- and few-synapse inputs, synapse removal would likely result in some decrease in the number of Purkinje cells innervated by a climbing fiber branch (i.e., its divergence). We thus compared the divergences of climbing fiber branches at P3 and P7 (Figures 3B and 3C). The distributions were not significantly different (Wilcoxon rank-sum test, $p = 0.99$). However, both of these histograms included information from climbing fiber branches with terminal arbors that were only partially contained inside the volume (that is, whose most distal branches ramified outside the volume boundary at some point); furthermore, the P3 and P7 image volumes were not identical in size. Both of these factors could obscure an actual change in the divergence between P3 and P7, especially if that change is subtle. To make a more reliable measurement, we removed from our analysis all climbing fiber branches whose terminal arbors left the volume (leaving 8/55 branches at P3 and 9/49 at P7; Figures 3D and 3E). The divergences for branches with complete terminal arbors also did not differ significantly between P3 and P7 (Wilcoxon rank-sum test, $p = 0.58$), arguing that climbing fiber branches remain connected to roughly the same number of Purkinje cells over these 4 days and were hence not undergoing net pruning. For this reason, we suspect that the smaller number of climbing fiber branches we observed to innervate the fully reconstructed P7 cell (49) relative to the P3 cell (55) is likely due to random variation in climbing fiber innervation and the different sizes of the datasets, rather than a systematic change in connectivity between these two ages.

To summarize, the main difference between the P3 and P7 datasets is that individual climbing fibers form significantly more synapses onto their Purkinje cell targets at P7 than at P3. Notably, the synapse addition process that occurs between these two ages appears to be preferential, because climbing fibers elaborate many synapses onto a small number of their Purkinje targets.

Strong and Weak Climbing Fiber Inputs to Purkinje Cells Have the Same Size Synapses

As shown by several studies, the extent of the postsynaptic density (PSD) can serve as a proxy for synaptic strength (Bailey and Chen, 1983, 1988a, 1988b; Bartol et al., 2015). We thus measured the PSD areas of all identified climbing fiber-Purkinje cell synapses at each age (STAR Methods; Figures 4A–4C). The PSD area distributions were significantly different between P3 and P7 (Figure 4D; $p \approx 0$, Wilcoxon rank-sum test). In particular, although the range of PSD areas overlapped, in the younger mouse the median PSD area was 1.4 times larger, and the variance was 4.9 times larger than at P7 (median: 0.22 μm^2, P3 versus 0.16 μm^2, P7; variance: 0.088 μm^2, P3 versus 0.018 μm^2, P7). One interpretation of this difference is that as the nervous system matures, synapse size becomes more consistent. To learn whether climbing fiber branches that form the smallest numbers of synapses onto a Purkinje cell (and may be more likely to be pruned) have PSD areas that differ significantly from climbing fiber branches that form large numbers of synapses onto a Purkinje cell (and hence may be more likely to remain), we measured the correlation between the PSD area of a synapse and the total number of synapses shared by its pre- and postsynaptic partners. We found that synaptic area was not correlated with the number of synapses formed between a climbing fiber and Purkinje cell (Figures 4E–4H; $p = 0.38$, P3; $p = 0.41$, P7; permutation tests, 100,000 permutations each). Taken together, these results show that individual

climbing fiber-to-Purkinje cell synapses are indistinguishable from a PSD perspective and suggest that the primary means by which a climbing fiber changes its efficacy is by altering synapse number.

Simulation: Synapse Addition Occurs via Preferential Attachment

To better understand the process by which the P3 connectivity pattern transformed into the pattern observed at P7, we constructed a time-stepping simulation to evolve the connectivity we observed at P3 (Figures 2C and 2E) to a state of connectivity similar to that at P7 (Figures 2D and 2F). The model (STAR Methods) allowed stochastic removal and addition of synapses by each climbing fiber branch with the Purkinje cells it was already connected to. Because we found that climbing fibers establish disproportionately large numbers of synapses onto subsets of their Purkinje targets, the model also controlled the probability of choosing a particular target cell for synapse addition. This probability was proportional to the number of synapses currently shared by the climbing fiber and Purkinje target. The exponent of this proportionality, γ, was varied to reflect a range of paradigms, from preferential attachment (positive γ), to no dependence ($\gamma = 0$), to penalization of strong inputs (negative γ). We varied γ and the relative rates of synapse addition and removal to test a range of potential models for climbing fiber-Purkinje cell synapse rewiring.

We went through this exercise to test in particular two different mechanisms that might produce the transformation between P3 and P7 connectivity. First, this transformation might occur through preferential attachment of climbing fibers to their target cells. Alternatively, the P7 result could potentially develop without preferential attachment if there were both non-selective addition ($\gamma = 0$) and elimination of synapses. In this case, the number of synapses shared by any climbing fiber-Purkinje cell pair would do a random walk over time about its P3 value. As a result, some pairs would “drift” toward larger numbers of shared synapses and other pairs would drift toward smaller numbers, causing a spread in the histogram of synapse numbers, which qualitatively is what we observed at P7. Importantly, it may also have been the case that neither of these mechanisms were sufficient to generate the observed changes in synaptic connectivity and that a more complex set of rules was required.

We found, however, that only preferential attachment processes could evolve P3 connectivity into P7-like connectivity (Figure 5A). Non-selective addition and removal of synapses always evolved the P3 distribution to one that was less like a power law and never converged toward the actual P7 distribution (Figures S6A–S6D). With preferential attachment, P3 connectivity evolved into a state statistically indistinguishable from P7 if the rate of synapse removal was zero or low (at least 2,000 times smaller than the rate of addition) and if γ was roughly in the range of 0.5 to 1.7. These parameter values suggest that removal of synapses is not a significant component of synapse rewiring between P3 and P7 (consistent with our studies of axonal divergence above). These values also argue that preferential synapse addition by climbing fibers onto their Purkinje targets is required to produce the disproportionately large numbers of synapses we observed at P7.

Using this model of preferential attachment, we could estimate rates of net climbing fiber synapse addition and removal that would lead to the connectivity we observed (Figures 5B

and 5C). For example, if we let the synapse removal rate be 5,000 times lower than the addition rate and $\gamma = 1.1$, the simulation took 955 ± 16 time steps to reach P7-like connectivity (mean ± SEM, 100 simulations). Because the simulation covered 4 days (P3 to P7), the average duration of a time step was 6 min. We thus calculated that individual climbing fiber branches added synapses at a median rate of one every 7 h and a maximum rate of one every hour. In this simulation, synapse removal was essentially absent over the 4 days.

Climbing Fiber Branch Morphology Can Be Used to Estimate the Number of Climbing Fibers that Innervate Developing Purkinje Cells

Above, we assessed the connectivity properties of all climbing fibers that innervated the fully reconstructed Purkinje cells in the P3 and P7 image volumes, where the climbing fibers were potentially split into multiple branches. Although much useful information can be revealed by studying these branches, more insight still can be obtained if the number of different fibers producing those branches is known. The direct way to get complete knowledge of the number of innervating climbing fibers would be to reconstruct these axons back to their entry points in the cerebellar peduncle. However, this task would require collecting image volumes that are intractably large at present (millimeters on a side, >10 petabytes of raw data). Instead, we estimated the number of different climbing fibers innervating the fully reconstructed Purkinje cell in our P7 dataset by building on our observed climbing fiber terminal arbormorphologies and results from previous anterograde labeling. Anterograde tracer studies have shown that in the first postnatal week, individual climbing fibers form multiple overlapping terminal arbors in the Purkinje cell layer (Sugihara, 2005). To calculate how many climbing fibers innervated one Purkinje cell, we needed to know how many terminal arbors provided innervation to that cell. However, because many of the innervating branches were incomplete, i.e., fragments of terminal arbors, our first step was to learn the number of branch fragments a terminal arbor could supply to the volume if it were not completely within the volume. To estimate this number, we spatially transposed climbing fiber terminal arbors by applying random (but constrained) translations to the 9 complete terminal arbors in our reconstruction (Figure 6A). We then computed the number of separate branches that those transposed arbors produced by leaving and re-entering the image volume (STAR Methods). Using this approach, we learned that a single terminal arbor is broken into1.8 branch fragments on average in the P7 volume (Figure 6B). Thus, the 49 climbing fiber branches that innervated the fully reconstructed Purkinje cell probably came from about 27 terminal arbors. Late in the first postnatal week, an individual climbing fiber extends 7.4×10^{-4} terminal arbors/μm^2 into each local region of cortex it innervates (from Sugihara, 2005; STAR Methods; Figures S6E–S6G), which given our 9,000 μm^2 Purkinje cell layer translates to 6.7 terminal arbors per climbing fiber in the P7 volume. At P7 we estimated that ~4 different climbing fibers (27/6.7)innervated the fully reconstructed Purkinje cell.

Our connectivity data also allowed us to compute how climbing fibers distributed their connectivity across the entire image volume. Given that 27 terminal arbors innervated the fully reconstructed Purkinje cell and that a single terminal arbor innervated on average 4 Purkinje cells in the volume (Figure 3E),we estimated that 203 terminal arbors innervated

the 30 Purkinje cells in the volume [(27 terminal arbors per Purkinje cell * 30 Purkinje cells)/(4 repetitions of each terminal arbor due to its divergence)]. Because a climbing fiber forms roughly 6.7 terminal arbors in this volume, we estimate that there are 30 different climbing fibers innervating the Purkinje cells in our dataset. This number corresponds to roughly one climbing fiber per Purkinje cell (Discussion).

Our estimates of 4 climbing fibers innervating a single Purkinje cell and 30 climbing fibers innervating all Purkinje cells in the volume give us information about the divergence of individual climbing fibers (as opposed to any of their individual terminal arbors). For 30 climbing fibers to innervate 30 Purkinje cells such that each Purkinje cell receives 4 climbing fiber inputs, each climbing fiber should have a divergence of 4 Purkinje cells (4 axons per Purkinje cell * 30 Purkinje cells = 120 innervations of Purkinje cells by axons, from 30 axons in the volume, thus each axon innervates 120/30 = 4 Purkinje cells). Notably, this value matches the average divergence of climbing fiber branches (Figure 3C). This information suggests that on average all branches of an individual climbing fiber restrict their innervation to the same (4) Purkinje cells (or subsets thereof).

Branches of the Same Climbing Fiber Have Shared Connectivity Preferences

After the first postnatal week, the synaptic preferences established by climbing fiber branches lead to eventual single innervation of Purkinje cells by climbing fibers. Thus, a whole climbing fiber (not to be confused with the single branches of climbing fibers; Figures 2C–2F) must choose among its Purkinje targets the one (or ones) it will remain in contact with into adulthood. The question we wished to answer is whether the branches of an individual climbing fiber are acting in concert or independently

We used hierarchical clustering to explore the Purkinje cell preferences of the reconstructed climbing fiber branches in our P7 dataset (STAR Methods; Figure 7). We analyzed branches that showed a synaptic preference for at least one Purkinje cell (by forming at least 17 synapses on a Purkinje cell, i.e., greater than the 90th percentile of the synapse distribution in Figures 2D; see Figure 7A). Our clustering analysis (Figure 7B) revealed three groups of climbing fiber branches with shared preferences at P7 (http://bit.ly/bbandrossP7cfgroups). All members of each group exhibited the same preferences for a subset of Purkinje cells. In particular, the branches in group 1 (IDs 59, 14, 7, and 15; Figure 7C) each innervated Purkinje cell 17 more strongly than any other, establishing a total of 105 synapses on this cell. The branches in group 2 (29, 4, 9, 13, 46, 5, and 37) each established the largest number of synapses onto Purkinje cell 25 (194 in total). The branches in group 3 (56, 3, and 72) all exhibited a synaptic preference for Purkinje cell 1 (the fully reconstructed cell), forming 61 synapses in total on that cell. The remaining branches we analyzed (31, 44, 67, 2, and 33) also showed preferences, but they did not co-share preferences for single Purkinje cells as strongly as the other groups did. The shared preferences among climbing fiber branches in a group for the same Purkinje cell were statistically unlikely to have occurred by chance (STAR Methods; $p = 0.004$). When we repeated this analysis at P3, we did not find groups of climbing fiber branches with significant shared Purkinje cell preferences ($p = 0.36$).

Thus, as climbing fiber branches form synapses over the first postnatal week, groups of them develop preferences for the same sets of Purkinje cells. These preferences do not appear to be a result of spatial factors, as we could find no topographical patterns to the sets of preferred cells for each group we identified at P7 (Figure 7D).

The climbing fiber branches with shared Purkinje cell preferences at P7 may be related in two ways: they might be branches of the same climbing fiber, or they might be branches from different fibers. We considered the likelihood of these relationships by again considering data about climbing fiber morphology and divergence. Above, we calculated that the 49 climbing fiber branches innervating the fully reconstructed Purkinje cell corresponded to ~4 climbing fibers. Thus, we expect that the 19 branches for which we assessed preferences originate from ~4 or fewer climbing fibers, because they all innervated the fully reconstructed Purkinje cell.

For branches of the same climbing fiber, we hypothesize that their synaptic preferences are similar, i.e., they fall into the same group. If they did not, then two things must occur to generate the results in Figure 7C: first, different branches of the same climbing fiber would have to exhibit different synaptic preferences; and second, subsets of branches from different climbing fibers would have to share the same preferences. We cannot conceive of a means of dividing branches in this way. Moreover, electrophysiological studies consistently show that during early postnatal development only one climbing fiber input becomes strong (Kano et al., 2018), which contradicts the idea of multiple axons having the same synaptic preferences.

These results lead to the conclusion that many branches of the same climbing fiber have similar synaptic preferences. We believe that because of this feature, it is possible to infer the origin climbing fiber for different branches based on their synaptic connectivity alone. This conclusion has important implications not only for cerebellar development but for connectomics in general (Discussion).

DISCUSSION

In this study, we produced electron microscopy image volumes of mouse cerebellum at P3 and P7 and reconstructed climbing fiber branches and their Purkinje cell targets in order to learn more about the changing organization of climbing fiber input to Purkinje cells in the first postnatal week. Our results reveal several features of climbing fiber-Purkinje cell synapse rearrangement. First, single climbing fibers (with branches working in concert) form many additional synapses to focus their innervation onto a subset of their Purkinje targets. Second, single-synapse strengths (measured by PSD area) become more uniform and do not correlate with the overall strength of a climbing fiber-Purkinje cell connection. These two points, combined with our confirmation that synaptic pruning does not occur, lead us to conclude that synapse addition is the primary mode of functional differentiation in the first postnatal week. This structural information is more consistent with electrophysiological evidence of synaptic strengthening in the first postnatal week (Hashimoto and Kano, 2003; Bosman et al., 2008) than results suggesting changes begin in the second week (Scelfo and Strata, 2005). Third, we infer that synapse addition between P3 and P7 involves positive

feedback between climbing fibers and Purkinje cells. This feedback appears to be nearly linear in nature and predicts that climbing fibers establish preferences by adding one synapse every 1 to few hours.

We also addressed a challenge that beset our analysis and is present in many other connectomic image volumes, i.e., that practically all axons are incomplete because connectomic volumes are small relative to neuron sizes. We combined information about large-scale climbing fiber morphology (Sugihara, 2005) with our own reconstructions of terminal arbors and their synaptic connectivity to quantify the total number of climbing fibers that innervated the 30 Purkinje cells in our P7 image volume. This information provides important context about climbing fiber-Purkinje cell synapse rearrangement: there appears to be parity between young climbing fibers and Purkinje cells. If detailed synaptic connectivity were not determined for our P7 dataset, a range of other scenarios could seem appropriate. In particular, because each Purkinje cell is innervated by 4 climbing fibers on average (Results), the maximum number of climbing fibers that could have innervated 30 Purkinje cells was ~120 (4 distinct axons per cell) and the minimum number is 4 (if the same 4 axons innervated every cell). The actual number of inputs, 30, is exactly what one would expect to find innervating a volume of 30 Purkinje cells in adult cerebellum, because adult climbing fibers innervate Purkinje cells sparsely, rarely innervating more than one cell in a field of 30. More specifically, an adult climbing fiber forms synapses with ~10 Purkinje cells out of thousands in a few cerebellar lobules (Sugihara et al., 2001; Fujita and Sugihara, 2013). Climbing fiber branching in development thus appears to be economical: the number of climbing fibers that innervate Purkinje cells in a local region in the first postnatal week is just enough to assure that each axon ends up with a postsynaptic target and that none branched there in vain.

This information, taken together, provides a glimpse at how development translates into structural changes in brain circuitry. It also provides useful constraints on the mechanisms that underlie developmental rewiring in this region of cerebellum.

Finally, although we studied synaptic connectivity from climbing fiber branches onto Purkinje cells, these electron microscopy volumes also contain ample information about all other cell types found in cerebellar cortex, their organelles, and their synaptic connectivity. These image volumes are thus useful resources for investigations of normal cerebellar development in mouse.

Branches of the Same Climbing Fiber Exhibit Similar Synaptic Preferences via a Contact-Mediated Mechanism

Our analysis indicates that groups of climbing fiber branches in the P7 volume had statistically significant similarities in their synaptic connectivity (Figure 7C). These similarities were not explained by close fasciculation of those branches. Indeed, each climbing fiber branch appeared to have a completely individual branching pattern (http://bit.ly/bbandrossP7cfgroups). Based on a number of arguments (Results), we think it likely that each such group originates from one climbing fiber. This finding leads to an important implication for the way that preferred Purkinje cells are chosen. Namely, climbing fibers do not establish synaptic preferences with a particular Purkinje cell through specific, directed

arborization during the first postnatal week. Rather, they establish large numbers of synapses at sites where they happen to be in contact. In this sense preferences are contact mediated rather than axon growth mediated. This idea is strengthened by the observation that climbing fiber branching is not pronounced in the vicinity of preferred cells compared with other Purkinje cells. Rather, the only evidence of the site of the preferred Purkinje cell is the greater density of synapses per axon length (http://bit.ly/bbandrossP3NGL, P3; http://bit.ly/bbandrossP7NGL, P7). One interpretation of this situation is that between P3 and P7 climbing fibers add synapses along existing branches that are already juxtaposed with a preferred Purkinje cell target.

This finding also illustrates an important point for connectomics datasets in general: namely, it may be possible to regroup broken axon pieces by leveraging their synaptic connectivity, as we have done for the P7 cerebellum dataset. This strategy should allow for more complete axonal reconstructions and therefore more accurate connectivity analysis. This type of connectivity-based inference is only possible with analysis in high-resolution connectomics datasets, in which all synapses formed by branches of an axon can be identified and their distributions across targets can be directly measured.

Functional Differentiation Differs between the Cerebellum and the NMJ

Our observations indicate that in the first postnatal week, climbing fibers develop preferences for certain Purkinje cells as they add synapses (Figures 7B and 7C). Based on the idea that multiple branches originate from the same climbing fiber (Results), there may be hundreds of synapses added by one climbing fiber onto one Purkinje cell between P3 and P7, while other climbing fibers innervating the same Purkinje cell change their synaptic input much more modestly. For example, the branches in group 1 of our preference analysis collectively form 105 synapses onto Purkinje cell 17, their preferred target, but only 4 synapses onto Purkinje cell 1, a non-preferred target. Given the loss of all but one input over the next few weeks and previous electrophysiology work (Hashimoto et al., 2011), it seems likely that the climbing fiber with the large increment in synapses will be the one that remains after synaptic rewiring is complete. Importantly, there was no evidence in our studies of synapse loss in the first postnatal week as strengthening occurred (Figures 3 and 5), although in later weeks massive elimination takes place (Kano et al., 2018).

This sequence of events for climbing fibers contrasts with developmental synapse rearrangement of motor axons at the NMJ, although in both cases postsynaptic targets are initially innervated by multiple axons and end up with a single axonal input. At the NMJ, multiple axons that converge undergo a process of synapse exchange: an axon adds synaptic territory by taking over space that was vacated by a different axon (Walsh and Lichtman, 2003; Gan and Lichtman, 1998; Turney and Lichtman, 2012). Synapse addition and loss are thus inextricably linked, with synapse loss appearing to be required for strengthening of the ultimate surviving input (a pattern also observed elsewhere: Chen and Regehr, 2000; Lichtman, 1980). Our results, however, provide evidence that early synaptic strengthening of climbing fiber inputs is unrelated to synapse removal by other fibers. A classical Hebbian mechanism may underlie the establishment of a dominant input in the cerebellum (Hebb, 1949; Kawamura et al., 2013; Lichtman and Balice-Gordon, 1990).

Persistence of Weak Climbing Fiber Inputs

The persistence of weak climbing fiber inputs despite the emergence of a dominant input during the first postnatal week raises the question of why these neurons would maintain weak connectivity. Physiologically effective climbing fibers in an adult establish many hundreds of synapses on a target cell, so it is unlikely that climbing fibers forming only a few synapses have functional significance. Axons may maintain weak connections to provide footholds on other target cells should the dominant input be damaged during development (Carrillo et al., 2013; Turney and Lichtman, 2012) or in case interactions between climbing fibers and Purkinje cells require a dominant input to refocus its resources elsewhere as has been proposed at the developing NMJ (Walsh and Lichtman, 2003). In this sense, Purkinje cells may be hedging their bets by remaining connected to multiple climbing fibers before the competition is resolved. From a climbing fiber perspective, the same may be true: an axon may remain connected to many targets to assure that it still innervates a few after most synaptic pruning has occurred.

Comparative Connectomics

Connectomics per se is a descriptive approach. It relies on inductive reasoning so that hypotheses are generated more easily than tested. One way, however, to generate and test hypotheses in connectomics datasets is to compare samples that differ in some way. In this study we have compared connectomics data from two developmental stages to learn how neural circuits become modified in early postnatal life. The power of this strategy is that a fundamentally static technique (looking at stained postmortem tissue) can be used to infer information about a highly dynamic phenomenon (the maturation of neural circuits). One challenge is that comparing connectomes is still a nascent approach. Although we possess potentially vast amounts of structural data from two time points, we do not yet know the ideal ways to make statistically rigorous comparisons. We contend that these two datasets contain material for an essentially unlimited number of hypotheses about how the cerebellum changes over the first postnatal week. Determining the best way to extract the things that are different and the things that are not from multiple samples will require turning these “digital tissues” into systematized databases that can be scrutinized automatically. This will likely be one of the central thrusts of connectomics going forward.

STAR★METHODS

LEAD CONTACT AND MATERIALS AVAILABILITY

Further information and requests for resources and reagents should be directed to and will be fulfilled by the Lead Contact, Alyssa Wilson (amw7@princeton.edu). This study did not generate new unique reagents or new unique mouse lines.

EXPERIMENTAL MODEL AND SUBJECT DETAILS

All animals were handled according to protocols approved by the Institutional Animal Care and Use Committee at Harvard University.

We prepared samples for electron microscopy from the cerebella of two CD1 wild-type unsexed mouse pups, one aged P3 and one aged P7, from different timed-pregnancy mothers

(Charles River). Cages were checked twice a day for pups (once in the morning and once in the evening) and P0 was assigned at the time when pups were found. Ages are thus accurate to within 12 hours.

METHOD DETAILS

Data Acquisition—We anesthetized pups with 0.01 mL of sodium pentobarbital (50 mg/mL) and intracardially perfused each with 2%–2% paraformaldehyde/glutaraldehyde in 0.15-M sodium cacodylate, 2-mM $CaCl_2$ buffer solution. We qualitatively monitored pup behavior to ensure that they behaved similarly to their littermates, and we measured brain sizes along the anteroposterior, mediolateral, and dorsoventral axes to ensure they fell within normal ranges. We then isolated the cerebellum from each sample and cut it into 300-μm-thick parasagittal sections. From each cerebellum, we chose one thick section in the medial part of the vermis (between 500 μm and 1 μm from the midline) and stained it using a ROTO protocol (Willingham and Rutherford, 1984) (2% osmium tetroxide plus 0.015 g/mL potassium ferrocyanide, 1% thiocarbohydrazide, and 2% osmium tetroxide). We then dehydrated and embedded each section in Epon 812 resin. We cut the embedded tissue into 30-nm sections using an automatic tape collecting ultramicrotome (ATUM) and post-stained each ultrathin section with 4% uranyl acetate and 4% lead citrate (Kasthuri et al., 2015).

We imaged these sections using secondary electron detection in a single-beam scanning electron microscope (1.7 kV; ZEISS Sigma). The acquisition was automated using WaferMapper software (Hayworth et al., 2014). Images were acquired at a resolution of 4 nm × 4 nm per pixel at a dwell time of 200 ns per pixel.

We reconstructed a Purkinje cell roughly in the middle of the P3 volume and one roughly in the middle of the P7 volume. In each case we also reconstructed all of its synaptic inputs. For each of the innervating axons we identified all of their other synapses and postsynaptic partners in the volume. We also reconstructed the somata of all the Purkinje cells in the volume at P3 and P7. Using this approach it was straightforward to identify a Purkinje cell as the synaptic target of an axon: starting from the postsynaptic density, we followed the target dendrite through the volume until it rejoined the cell soma. We used a similar approach to determine the identities of other synaptic targets in our reconstructions: starting at the postsynaptic density of a synapse, we followed the dendrite throughout the volume until it joined a cell soma. We then traced that soma, its axon and dendrites outward until we could determine its cell type. Most of this reconstruction was done by computer assisted manual tracing using the VAST-lite tool (Berger et al., 2018). In the P7 volume we began with a machine learning based segmented subvolume (72 μm × 72 μm × 30 μm) generated by Rhoana (Kaynig et al., 2015) and edited it using Mojo software (Knowles-Barley et al., 2013). The axon branches and cells in the subvolume were then extended throughout the volume using VAST.

Because our goal was to analyze the climbing fiber input to Purkinje cells it was important to classify each presynaptic axon branch in order to exclude axons that were not climbing fibers. We therefore determined the ultrastructural characteristics of the synapses it formed (excitatory versus inhibitory) to rule out inhibitory axons (i.e., Purkinje cell collaterals, stellate, basket, Golgi, Lugaro, and candelabrum cells; Palay and Chan-Palay, 1974;

Lainéand Axelrad, 1994). Inhibitory axons were identified by their lack of a pronounced postsynaptic density, a feature of excitatory synapses (Peters et al., 1991). Inhibitory synapses also possessed irregularly shaped vesicles (unlike the round vesicles we observed in excitatory axons). If a synapse was ambiguous we traced the axon to one or more additional synapses and this allowed an unambiguous determination of whether it was excitatory or inhibitory. We also could rule out excitatory granule cell axons by their distinctive morphology (i.e., a smooth, unbranched axon segment that ran parallel to many other similar axon segments along the mediolateral axis in the molecular layer, a feature of the parallel fiber portion of a granule cell axon; see Palay and Chan-Palay, 1974). We also excluded any axon that could be traced back to its cell body because climbing fibers originate outside the cerebellum, in the inferior nuclear olive (this allowed us to classify and remove inputs that were the radial ascending branch of a granule cell). The remaining excitatory axon branches were either climbing fibers, or mossy fibers (which originate in various nuclei outside the cerebellum as well as from recurrent collaterals of excitatory cells in the deep cerebellar nuclei inside the cerebellum, and from unipolar brush cell axons within the cerebellar cortex; see Hess 1982; Mugnaini and Floris, 1994; Mugnaini et al., 2011).

Because mossy fibers have been reported to make transient connections on Purkinje cells in development (Mason and Gregory, 1984; Kalinovsky et al., 2011), it was important to exclude these excitatory inputs to Purkinje cells as well. We therefore analyzed a subset of excitatory (non-granule cell) axon branches to identify all of their postsynaptic targets at both P3 (20 branches) and P7 (14 branches). We did this painstaking analysis in order to learn whether mossy and climbing fibers had different connectivity profiles. At each age we computed the fraction of synapses formed by these axon branches onto (1) Purkinje cells, (2) granule cells, and (3) interneurons. At both ages we found a clear splitting of branches into two groups (Figure S2): branches that formed a much larger fraction of their synapses onto Purkinje cells relative to granule cells, and branches that formed a much larger fraction of their synapses onto granule cells relative to Purkinje cells.

Based on this preliminary result, we attempted to find a quantitative criterion to split the climbing fibers from the putative mossy fibers. We therefore wrote code to perform two modes of cluster analysis (k-means and hierarchical agglomerative clustering; http://bit.ly/bbandrosskhclust) to group the branches we analyzed based on their connectivity properties. Along with data for these axon branches, at each age we also included a set of axons we identified separately from the inputs to each fully reconstructed Purkinje cell, and that we believe are definitely mossy fibers (12 at P3 and 10 at P7). These axon branches innervated the dendrites of granule cells deep in the internal granular layer, which is a synapse type characteristic of mossy fibers, and not of climbing fibers (see e.g., Ito and Takeichi, 2009). Often these axon branches also formed large, amorphous synaptic boutons with the granule cell dendrites they innervated, in a configuration that resembled the well described mossy fiber rosette (Ramón y Cajal, 1995; Palay and Chan-Palay, 1974). These mossy fiber branches were used (1) to validate whether our clustering based on synaptic connectivity could separate climbing fibers and mossy fibers and (2), if so, to help us identify which group of axons contained mossy fibers and which contained climbing fibers. Both clustering methods produced nearly the same classification metric (see Figure S2; Tables S2 and S3).

Based on this analysis, the axon branches could be completely separated into types. At P3 axon branches that formed at least 40% of their synapses with Purkinje cells (they formed the rest with interneurons and rarely with granule cells) were a distinct class from the other axons that we sampled which made larger numbers of synapses with granule cells and very few synapses with Purkinje cells. This latter group clustered with the actual mossy fibers we identified. Thus we think that this clustering allowed us to exclude mossy fibers from our climbing fiber population. At P7 the same approach clustered the climbing fibers by choosing branches that formed at least 70% of their synapses on Purkinje cells. At both ages, as our threshold for identifying climbing fibers, we used the largest fraction of synapses formed onto Purkinje cells that separated the climbing fiber cluster from the mossy fiber cluster, rounded up to the nearest tenth. In this way, we made our criterion for identifying climbing fiber branches in each dataset slightly more stringent. We excluded any axon that established fewer than 5 synapses in the volume from our analysis. In the P7 dataset, we also excluded two axon branches that formed 9 synapses each in the volume but only ramified for short distances within the Purkinje cell layer, since it was unclear how their connectivity profiles might change if more of those axon branches were visible.

The P3 and P7 image volumes and segmentations are freely available at https://bossdb.org/project/wilson2019.

Checks on Dataset Suitability—We took several steps to ensure that our datasets represent connectivity from typical, wild-type CD1 mice. First, we recorded the appearance, behavior, and brain size of the mice used to generate our P3 and P7 datasets and found them to be consistent with normal values (see above). Second, we measured the thicknesses of the cortical layers in the P3 and P7 datasets and found them to be consistent with previously reported values: from Figure S1A, at P3 we measure an EGL thickness of ~30 μm, ML of ~10 μm, and PCL of ~30 μm to 35 μm. At P7, we measured an EGL of ~50 μm, ML of ~15 μm, and PCL of ~20 μm. (Compare with Martinez et al., 2013 and the Allen Brain Atlas for developing mouse, in particular with layers of cerebellar vermis in lobule VIII shown with calbindin labeling of Purkinje cells at P4: http://developingmouse.brain-map.org/experiment/show/100031932, where EGL+ML ~60 μm, PCL ~33 μm. See also Leto et al. (2016), where in Figure 15 the P7 vermis has an EGL of ~45 μm thickness, ML of ~25 μm, and PCL of ~25 μm.) Third, the sizes and morphologies of the Purkinje cells in our datasets were consistent with previous reports (compare Figure S1 with Figure 7A in Sotelo, 2004).

Several connectivity properties we measured in our datasets also indicate that the mice we used could be considered typical. First, the climbing fiber synaptic connectivity distributions for all Purkinje cells sampled at both ages were well described by power laws (Figure 2); if either mouse used for our datasets had been affected by irregularities in connectivity, we would predict that they would not have shown the same type of distribution across the Purkinje cells in both mice. (We also note that each mouse originated from a separate timed-pregnancy mother and that they were born two years apart, so it is unlikely that both mice would be affected by the same abnormality.) Second, we estimate that 4 climbing fibers on average innervate a single Purkinje cell at P7 (see Results and Figure 6), which is consistent with previous reports stating that 5 or fewer climbing fibers innervate each Purkinje cell in the first postnatal week (Hashimoto and Kano, 2003; Crepel et al., 1976). Third, we found

no evidence that climbing fibers were being removed from Purkinje cells between P3 and P7 (Figures 3B–3E), which is consistent with previous reports from electrophysiology experiments (see Kano et al., 2018 for a review).

QUANTIFICATION AND STATISTICAL ANALYSIS

Power Law Fits—Fits were computed for the synapse distributions (number of synapses formed by single climbing fiber branches onto each Purkinje cell they innervated) using the scipy.optimize.curve_fit function in Python.

Climbing Fiber Length and Synapse Density—Skeletons were computed for climbing fiber branches in both datasets using Kimimaro (https://github.com/seung-lab/kimimaro) and Igneous (https://github.com/seung-lab/igneous) software and can be viewed in Neuroglancer (https://github.com/amwilson149/baby-andross). The total length of each branch was queried with this software using the cable_length attribute for these skeletons. To compute the length of each climbing fiber branch that was in the Purkinje cell layer, we cropped the skeletons to include only the pieces above the Purkinje cell layer-internal granular layer interface (i.e., the pieces in the upper 75% of the volume at each age) and then computed the cable length. Synapse densities in the Purkinje cell layer were computed by dividing the total number of synapses formed by a climbing fiber branch onto Purkinje cells in the Purkinje cell layer by the total length of the branch in the Purkinje cell layer. See Figure S4.

Postsynaptic Density Area—We manually traced the PSDs of all the climbing fiber segment-Purkinje cell synapses using VAST. To accurately represent PSD shapes with these annotations, we converted voxel lists from pixel values (which were anisotropic: 4 nm/px × 4 nm/px × 30 nm/px) to units of nm. We then performed principal component analysis on each voxel list and used the third component to define the normal to the flattest plane of the PSD. We then projected the PSD voxel list onto this plane to create a 2-dimensional version of the PSD. We computed the convex hull of the projected pixels and used it to compute an estimate of the PSD area. This method was insensitive to factors like the orientation of a PSD within the image volume.

Time-Evolution Simulation—We wrote a simulation to evolve synaptic connectivity matrices using stochastic synapse addition and removal in order to explore the types of processes that could generate the connectivity observed at P7, given an initial connectivity identical to what we observed at P3. In the simulation the connectivity matrix was initialized to the observed P3 connectivity (i.e., 55 rows × 30 columns with values producing the distributions in Figure 2C). A target connectivity matrix was set to the observed connectivity at P7 (49 rows × 18 columns with values producing the synapse distribution in Figure 2D). For both ages, the first column represented the connectivity by climbing fiber branches onto the fully reconstructed Purkinje cell.

In each timestep, we (1) removed a synapse from several randomly chosen connected climbing fiber branch-Purkinje cell pairs (i.e., we decremented the values of several nonzero connectivity matrix elements). We then (2) compressed the connectivity matrix by (a)

removing climbing fiber branches that became completely disconnected from the Purkinje cells in our dataset (rows containing only zeros), (b) removing Purkinje cells that became completely disconnected from the climbing fiber branches in our dataset (columns containing only zeros), and (c) removing climbing fiber branches that were no longer synaptically connected to the fully reconstructed Purkinje cell (rows for which the element in the first column became zero). We removed the rows that met condition (c) so that the connectivity matrix always reflected what we would have measured by reconstructing circuitry as we did in our P3 and P7 datasets (i.e., by identifying the climbing fiber synaptic inputs to one fully reconstructed Purkinje cell and then adding connectivity information for all the other Purkinje cells they innervated in the volume). We then (3) added synapses at several randomly chosen climbing fiber segment-Purkinje cell interfaces (i.e., incremented the value of some nonzero matrix elements). Finally, we (4) compared the resulting connectivity matrix with the target matrix to determine whether the two were statistically indistinguishable (see below). If they were, we regarded this time step as one in which P7-like synaptic connectivity had been reached. The software we developed for this purpose can be found here (along with a description of the parameters): http://bit.ly/bbandrossevolve.

To determine whether a simulated connectivity matrix was statistically indistinguishable from the target matrix, we compared the two using four features: (1) the full synapse distribution (number of synapses per climbing fiber branch onto each of its Purkinje cell targets), (2) the distribution of total number of synapses formed by each climbing fiber branch (row-wise weight distribution), (3) the distribution of the number of Purkinje cells innervated by each climbing fiber (i.e., climbing fiber divergence, or row-wise weight density), and (4) the distribution of the number of climbing fibers innervating each Purkinje cell (i.e., climbing fiber convergence onto Purkinje cells, a measure of column-wise weight density). We also tracked the sizes of the matrices (i.e., the number of climbing fiber branches (rows) and the number of Purkinje cells (columns)) and required them to not become more different than the size difference between P3 and P7. However, the sizes could be derived from (1) and (2) above, so these measurements were not independent constraints on the simulation. Rather, we used them as a sanity check.

We considered properties (1) through (4) for the simulated and P7 matrices to be statistically indistinguishable if a Wilcoxon rank sum test failed to detect a difference at an alpha level of 0.05. We required all of these properties to be statistically indistinguishable for the simulated matrix to be considered as having reached the actual P7 configuration.

Number of Branches per Terminal Arbor—To estimate the number of branches that a climbing fiber terminal arbor extended into our image volumes, we used our reconstructions of unbroken climbing full terminal arbors at P7 (9/49 branches) as templates and simulated how similar arbors could be broken by crossing the image volume boundaries. For each simulation we randomly selected a terminal arbor from this reconstructed set with replacement. We then applied randomly chosen but constrained translations to the voxel list for that terminal arbor. Within the Purkinje cell layer (i.e., the x-z plane), we allowed translations in any direction by any amount (with uniform probability) that ranged from zero up to a displacement of 120 μm (the volume width) in x and up to 75 μm (the volume depth) in z. A terminal arbor at the maximum displacement in either dimension would thus be

located just outside the volume. We also allowed translations in either direction along the y axis of up to 2 μm to allow varying arbor positions while enforcing the biological constraint that climbing fiber terminal arbors should terminate in the Purkinje cell layer. We then applied the bounding box of the image volume ((0 μm, 0 μm, 0 μm) to (120 μm, 190 μm, 75 μm)) to the resulting voxel list. Specifically, any voxel of a simulated terminal arbor that fell outside the image volume was removed, to reflect the fact that that portion of the arbor would not have been reconstructed. For the remaining voxels we then counted the number of connected components. We repeated this process 500 times to produce a distribution of the number of branches produced by broken terminal arbors in the P7 image volume.

Climbing Fiber Terminal Arbor Density—We computed the number of terminal arbors extended per climbing fiber axon in a single microzone of cerebellar cortex (usually a part of a lobule) during the first postnatal week using measurements reported in Figures 1B and 6A of Sugihara (2005). In that report, images of dye-labeled rat climbing fibers and the majority of their terminal arbors were presented, along with the number of terminal arbors extended by those climbing fibers into the cerebellar cortex. We estimated densities of 8.7×10^{-4} terminal arbors/μm^2, 9.8×10^{-4} terminal arbors/μm^2, and 2.99×10^{-4} terminal arbors/μm^2 in lobules II, III, and crus Ic, respectively, from the P6 rat in Figure 1B and 8×10^{-4} terminal arbors/μm^2 in lobule VIb-c from the P5 rat in Figure 6A, in the transverse plane of the cerebellar cortex (i.e., the plane parallel to the Purkinje cell layer). We note that the densities measured in vermal regions are similar to each other but roughly 3 times the density measured in the hemispheric region (crus Ic). This information suggests that the vermal estimates might be more appropriate for our lobule VIII vermis data. However, in the absence of more complete information about the variation in climbing fiber terminal arbor density with cerebellar location, we took the approach of including all the density estimates available from Sugihara (2005) in our analysis.

Although these densities were measured for rat climbing fibers, reconstructions of mouse climbing fibers at the same time point (there is evidence that mice and rats are age-matched to within a day or so in their cerebellar postnatal development timeline–see e.g., Kano et al., 2018) appear to have similar terminal arbor densities. Specifically, our measurements of terminal arbor densities in P5 and P6 rat from Sugihara (2005) correspond to average distances between neighboring terminal arbors of 35 μm, 33 μm, 35 μm, and 50 μm in lobules II, III, VI, and crus 1b-c, respectively. A reconstruction of a P5 mouse climbing fiber performed by Mason and Gregory (1984) shows distances of 40 μm and 50 μm between neighboring terminal arbors (cerebellar location unspecified; see Figure 8 of that paper). For this reason we felt it was reasonable to use the more abundant terminal arbor densities from Sugihara (2005) in our estimations.

The area in the transverse plane of the P7 volume is 9,000 μm^2. A single olivocerebellar axon with average terminal arbor density (7.4×10^{-4} terminal arbors/μm^2, computed from the estimates above) that fully overlapped the P7 image volume would thus extend 6.7 terminal arbors into the volume.

Grouping by Purkinje Cell Preference—We attempted to group climbing fiber branches by the similarity of their synaptic connectivity onto the Purkinje cells in the

volume at P3 and P7. We restricted our analysis to those branches that had strong preferences for at least one Purkinje cell. We considered a climbing fiber branch to have a strong preference if it formed a number of synapses onto at least one cell that was in the top 10th percentile of the connection sizes we observed (i.e., more than 3 synapses at P3 and more than 16 synapses at P7; Figures 2C and 2D, respectively). This population consisted of 23 climbing fiber branches at P3 and 19 branches at P7. For this population of climbing fiber branches, we treated the connectivity for each branch onto the Purkinje cells they innervated (a row of the connectivity matrix) as a feature vector, and computed the Euclidean distance matrix for the normalized feature vectors. The (i,j)-th element of the distance matrix represents how different the connectivity onto all Purkinje cells is for climbing fiber branches i and j. We then used hierarchical agglomerative clustering (see, e.g., James et al., 2013, Chapter 10) to group the climbing fiber branches according to this distance metric.

Significance Testing of Climbing Fiber-Purkinje Cell Connectivity Patterns— We used Monte Carlo simulations, resampling tests, and permutation tests to determine whether the various properties we observed could have resulted from random synaptic connectivity. These properties were (1) the distributions of the number of synapses formed by climbing fiber branches onto individual Purkinje cells in each dataset, (2) the correlations between PSD area of a synapse and the total number of synapses formed by its presynaptic climbing fiber branch onto its postsynaptic Purkinje cell, and (3) the ordering of climbing fiber branches into groups with shared Purkinje cell preferences, based on the numbers of synapses they formed onto each Purkinje cell target in our dataset.

For (1) the synapse number distributions, we performed a Monte Carlo simulation of the case where each climbing fiber branch formed synapses onto all its Purkinje cell targets with uniform probability. In each iteration of the simulation, we held the total number of synapses formed by each climbing fiber branch fixed at observed values, and required that the climbing fiber branch could only form synapses onto its observed Purkinje cell targets. For each synapse formed by the climbing fiber branch we chose the identity of the Purkinje target from the set of observed Purkinje cell targets, with replacement, according to a uniform probability distribution. We then computed the median and skewness of the resulting connectivity distribution. We repeated this simulation 100,000 times and compared the resulting median and skewness distributions with the observed values by computing p values at a significance level of 0.05 (Figure S3).

For (2) the PSD area correlations, we performed a permutation test to simulate how PSD area would relate to number of synapses for single climbing fiber branch-Purkinje cell pairs if they actually had a random relationship. In each iteration, we randomly permuted PSD areas for all climbing fiber branch-Purkinje cell synapses and computed the Pearson's correlation coefficient. We repeated this procedure 100,000 times and compared the resulting correlation distribution against the observed value by computing a p value at a significance level of 0.05.

To test (3) the significance of the groupings of climbing fiber branches based on Purkinje cell preferences, we performed a resampling test to simulate the condition in which climbing fibers established synaptic preferences onto random Purkinje cells among their observed

targets. In each iteration of the resampling test we kept the identities of the Purkinje cells innervated by each climbing fiber branch fixed at observed values. Then, for each climbing fiber branch, we randomly sampled the number of synapses formed onto each of its targets from the observed synapse distribution (Figures 2C and 2D), with replacement. We only assessed ordering in our observed data for climbing fiber branches that formed a number of synapses onto one or more Purkinje cell targets that were in the top 10th percentile of the connectivity distribution. Thus, in order to make sure that the resampled distribution always contained at least one many-synapse connection, we repeated the resampling process for each climbing fiber branch until the above requirement was satisfied. We then ordered the climbing fiber branches with resampled connectivity using hierarchical clustering. We measured the tightness of the resulting clusters by computing the standard deviation of the distribution of distances between linked groups (i.e., the lengths of the vertical lines in Figure 7B). At each age we generated 10,000 resampled distributions in this way and compared the corresponding observed values by computing p values at a significance level of 0.05.

DATA AND CODE AVAILABILITY

Scripts for Analysis—Scripts were written in Python 3.6, and can be found here (along with a list of package requirements): https://github.com/amwilson149/baby-andross.

Dataset Hosting—Electron microscopy data and annotations are stored on Johns Hopkins University Applied Physics Laboratory's BOSS (https://bossdb.org/project/wilson2019). Raw data will be made available on Mendeley under the project title "Electron-Microscopy-Based Synaptic Connectivity in Early Postnatal Mouse Cerebellum" (https://doi.org/10.17632/jsjny43yzz.1). A list of target URLs for the shortened links presented in this work are available on the Mendeley project page.

Supplementary Material

Refer to Web version on PubMed Central for supplementary material.

ACKNOWLEDGMENTS

We thank Daniel Berger, Daphna Keidar, and Will Silversmith for helpful discussions and thank those who helped with annotating the datasets (Silvia Caminiti, Lena Jiang, Jasmine Lopez, Brenda Marin-Rodriguez, Molly McGowan, Renuka Nannapaneni, Bryan Nelson, Stephen Ng, and Vinutna Veeragandham). We gratefully acknowledge support from the NIH/NINDS (National Research Service Award F31NS089223, 1DP2OD006514-01, TR01 1R01NS076467-01, 1U01NS090449-01, and U19NS104653); the Broad Institute (6600029-5500000959); the National Defense Science and Engineering Graduate (NDSEG) Fellowship Program; Conte (1P50MH094271-01); MURI Army Research Office (contract no. W911NF1210594 and IIS-1447786); NSF (OIA-1125087 and IIS-1110955); the Human Frontier Science Program (RGP0051/2014); the NIH and NIGMS via the National Center for Multiscale Modeling of Biological Systems (P41GM10371); and IARPA contract D16PC00002.

REFERENCES

Armengol JA, and Sotelo C (1991). Early dendritic development of Purkinje cells in the rat cerebellum. A light and electron microscopic study using axonal tracing in 'in vitro' slices. Brain Res. Dev. Brain Res 64, 95–114. [PubMed: 1786652]

Bailey CH, and Chen M (1983). Morphological basis of long-term habituation and sensitization in Aplysia. Science 220, 91–93. [PubMed: 6828885]

Bailey CH, and Chen M (1988a). Long-term memory in Aplysia modulates the total number of varicosities of single identified sensory neurons. Proc. Natl. Acad. Sci. USA 85, 2373–2377. [PubMed: 3353385]

Bailey CH, and Chen M (1988b). Long-term sensitization in Aplysia increases the number of presynaptic contacts onto the identified gill motor neuron L7. Proc. Natl. Acad. Sci. USA 85, 9356–9359. [PubMed: 2461569]

Barabási A-L, and Albert R (1999). Emergence of scaling in random networks. Science 286, 509–512. [PubMed: 10521342]

Bartol TM Jr., Bromer C, Kinney J, Chirillo MA, Bourne JN, Harris KM, and Sejnowski TJ (2015). Nanoconnectomic upper bound on the variability of synaptic plasticity. eLife 4, e10778. [PubMed: 26618907]

Berger DR, Seung HS, and Lichtman JW (2018). VAST (Volume Annotation and Segmentation Tool): efficient manual and semi-automatic labeling of large 3D image stacks. Front. Neural Circuits 12, 88. [PubMed: 30386216]

Bosman LW, Takechi H, Hartmann J, Eilers J, and Konnerth A (2008). Homosynaptic long-term synaptic potentiation of the “winner” climbing fiber synapse in developing Purkinje cells. J. Neurosci 28, 798–807. [PubMed: 18216188]

Carrillo J, Nishiyama N, and Nishiyama H (2013). Dendritic translocation establishes the winner in cerebellar climbing fiber synapse elimination. J. Neurosci 33, 7641–7653. [PubMed: 23637158]

Chedotal A, and Sotelo C (1993). The ‘creeper stage’ in cerebellar climbing fiber synaptogenesis precedes the ‘pericellular nest’–ultrastructural evidence with parvalbumin immunocytochemistry. Brain Res. Dev. Brain Res 76, 207–220. [PubMed: 8149587]

Chen C, and Regehr WG (2000). Developmental remodeling of the retinogeniculate synapse. Neuron 28, 955–966. [PubMed: 11163279]

Crepel F, Mariani J, and Delhaye-Bouchaud N (1976). Evidence for a multiple innervation of Purkinje cells by climbing fibers in the immature rat cerebellum. J. Neurobiol 7, 567–578. [PubMed: 1003202]

Fujita H, and Sugihara I (2013). Branching patterns of olivocerebellar axons in relation to the compartmental organization of the cerebellum. Front. Neural Circuits 7, 3. [PubMed: 23382711]

Gan W-B, and Lichtman JW (1998). Synaptic segregation at the developing neuromuscular junction. Science 282, 1508–1511. [PubMed: 9822385]

Hashimoto K, and Kano M (2003). Functional differentiation of multiple climbing fiber inputs during synapse elimination in the developing cerebellum. Neuron 38, 785–796. [PubMed: 12797962]

Hashimoto K, and Kano M (2013). Synapse elimination in the developing cerebellum. Cell. Mol. Life Sci 70, 4667–4680. [PubMed: 23811844]

Hashimoto K, Ichikawa R, Kitamura K, Watanabe M, and Kano M (2009). Translocation of a “winner” climbing fiber to the Purkinje cell dendrite and subsequent elimination of “losers” from the soma in developing cerebellum. Neuron 63, 106–118. [PubMed: 19607796]

Hashimoto K, Tsujita M, Miyazaki T, Kitamura K, Yamazaki M, Shin H-S, Watanabe M, Sakimura K, and Kano M (2011). Postsynaptic P/Q-type Ca2+ channel in Purkinje cell mediates synaptic competition and elimination in developing cerebellum. Proc. Natl. Acad. Sci. USA 108, 9987–9992. [PubMed: 21628556]

Hayworth KJ, Morgan JL, Schalek R, Berger DR, Hildebrand DGC, and Lichtman JW (2014). Imaging ATUM ultrathin section libraries with WaferMapper: a multi-scale approach to EM reconstruction of neural circuits. Front. Neural Circuits 8, 68. [PubMed: 25018701]

Hebb DO (1949). The Organization of Behavior: A Neuropsychological Theory (Wiley).

Hess DT (1982). Cerebellar nucleo-cortical neurons projecting to the vermis of lobule VII in the rat. Brain Res. 248, 361–366. [PubMed: 7139282]

Ito S, and Takeichi M (2009). Dendrites of cerebellar granule cells correctly recognize their target axons for synaptogenesis *in vitro*. Proc. Natl. Acad. Sci. USA 106, 12782–12787. [PubMed: 19622730]

Iwasaki S, and Takahashi T (2001). Developmental regulation of transmitter release at the calyx of Held in rat auditory brainstem. J. Physiol. 534, 861–871. [PubMed: 11483715]

James G, Witten D, Hastie T, and Tibshirani R (2013). An Introduction to Statistical Learning with Applications in R (Springer).

Kalinovsky A, Boukhtouche F, Blazeski R, Bornmann C, Suzuki N, Mason CA, and Scheiffele P (2011). Development of axon-target specificity of ponto-cerebellar afferents. PLoS Biol. 9, e1001013. [PubMed: 21346800]

Kano M, Watanabe T, Uesaka N, and Watanabe M (2018). Multiple phases of climbing fiber synapse elimination in the developing cerebellum. Cerebellum 17, 722–734. [PubMed: 30009357]

Kasthuri N, Hayworth KJ, Berger DR, Schalek RL, Conchello JA, Knowles-Barley S, Lee D, Vázquez-Reina A, Kaynig V, Jones TR, et al. (2015). Saturated reconstruction of a volume of neocortex. Cell 162, 648–661. [PubMed: 26232230]

Kawamura Y, Nakayama H, Hashimoto K, Sakimura K, Kitamura K, and Kano M (2013). Spike timing-dependent selective strengthening of single climbing fibre inputs to Purkinje cells during cerebellar development. Nat. Commun 4, 2732. [PubMed: 24225482]

Kaynig V, Vázquez-Reina A, Knowles-Barley S, Roberts M, Jones TR, Kasthuri N, Miller E, Lichtman J, and Pfister H (2015). Large-scale automatic reconstruction of neuronal processes from electron microscopy images. Med. Image Anal. 22, 77–88. [PubMed: 25791436]

Knowles-Barley S, Roberts M, Kasthuri N, Lee D, Pfister H, and Lichtman JW (2013). Mojo 2.0: Connectome Annotation Tool (Front Neuroinformatics).

Lainé J, and Axelrad H (1994). The candelabrum cell: a new interneuron in the cerebellar cortex. J. Comp. Neurol 339, 159–173. [PubMed: 8300903]

Leto K, Arancillo M, Becker EB, Buffo A, Chiang C, Ding B, Dobyns WB, Dusart I, Haldipur P, Hatten ME, et al. (2016). Consensus paper: cerebellar development. Cerebellum 15, 789–828. [PubMed: 26439486]

Lichtman JW (1980). On the predominantly single innervation of submandibular ganglion cells in the rat. J. Physiol. 302, 121–130. [PubMed: 7411451]

Lichtman JW, and Balice-Gordon RJ (1990). Understanding synaptic competition in theory and in practice. J. Neurobiol 21, 99–106. [PubMed: 2181069]

Mariani J, and Changeux JP (1981). Ontogenesis of olivocerebellar relationships. II. Spontaneous activity of inferior olivary neurons and climbing fibermediated activity of cerebellar Purkinje cells in developing rats. J. Neurosci 1, 703–709. [PubMed: 7346579]

Martinez S, Andreu A, Mecklenburg N, and Echevarria D (2013). Cellular and molecular basis of cerebellar development. Front. Neuroanat 7, 18. [PubMed: 23805080]

Mason CA, and Gregory E (1984). Postnatal maturation of cerebellar mossy and climbing fibers: transient expression of dual features on single axons. J. Neurosci 4, 1715–1735. [PubMed: 6737039]

Mugnaini E, and Floris A (1994). The unipolar brush cell: a neglected neuron of the mammalian cerebellar cortex. J. Comp. Neurol 339, 174–180. [PubMed: 8300904]

Mugnaini E, Sekerková G, and Martina M (2011). The unipolar brush cell: a remarkable neuron finally receiving deserved attention. Brain Res. Brain Res. Rev 66, 220–245.

Newman MEJ (2005). Power laws, Pareto distributions and Zipf's law. Contemp. Phys. 46, 323–351.

Palay SL, and Chan-Palay V (1974). Cerebellar Cortex: Cytology and Organization (Springer-Verlag).

Peters A, Palay SL, and Webster H. deF. (1991). Fine Structure of the Nervous System: Neurons and Their Supporting Cells, 3rd Edition (Oxford University Press).

Ramón y Cajal S (1995). Histology of the Nervous System of Man and Vertebrates (Oxford University Press).

Scelfo B, and Strata P (2005). Correlation between multiple climbing fibre regression and parallel fibre response development in the postnatal mouse cerebellum. Eur. J. Neurosci. 21, 971–978. [PubMed: 15787703]

Slater CR (2017). The structure of human neuromuscular junctions: some unanswered molecular questions. Int. J. Mol. Sci 18, e2183. [PubMed: 29048368]

Sotelo C (2004). Cellular and genetic regulation of the development of the cerebellar system. Prog. Neurobiol 72, 295–339. [PubMed: 15157725]

Sugihara I (2005). Microzonal projection and climbing fiber remodeling in single olivocerebellar axons of newborn rats at postnatal days 4–7. J. Comp. Neurol 487, 93–106. [PubMed: 15861456]

Sugihara I, Wu H-S, and Shinoda Y (2001). The entire trajectories of single olivocerebellar axons in the cerebellar cortex and their contribution to Cerebellar compartmentalization. J. Neurosci 21, 7715–7723. [PubMed: 11567061]

Tapia JC, Wylie JD, Kasthuri N, Hayworth KJ, Schalek R, Berger DR, Guatimosim C, Seung HS, and Lichtman JW (2012). Pervasive synaptic branch removal in the mammalian neuromuscular system at birth. Neuron 74, 816–829. [PubMed: 22681687]

Turney SG, and Lichtman JW (2012). Reversing the outcome of synapse elimination at developing neuromuscular junctions *in vivo*: evidence for synaptic competition and its mechanism. PLoS Biol. 10, e1001352. [PubMed: 22745601]

Walsh MK, and Lichtman JW (2003). In vivo time-lapse imaging of synaptic takeover associated with naturally occurring synapse elimination. Neuron 37, 67–73. [PubMed: 12526773]

Willingham MC, and Rutherford AV (1984). The use of osmium-thiocarbohydrazide-osmium (OTO) and ferrocyanide-reduced osmium methods to enhance membrane contrast and preservation in cultured cells. J. Histochem. Cytochem 32, 455–460. [PubMed: 6323574]

Highlights

- Climbing fibers begin functional differentiation by preferential synapse addition
- Synapse sizes of strong and weak climbing fiber inputs are indistinguishable
- Local over-innervation is economical: every climbing fiber can remain in adulthood

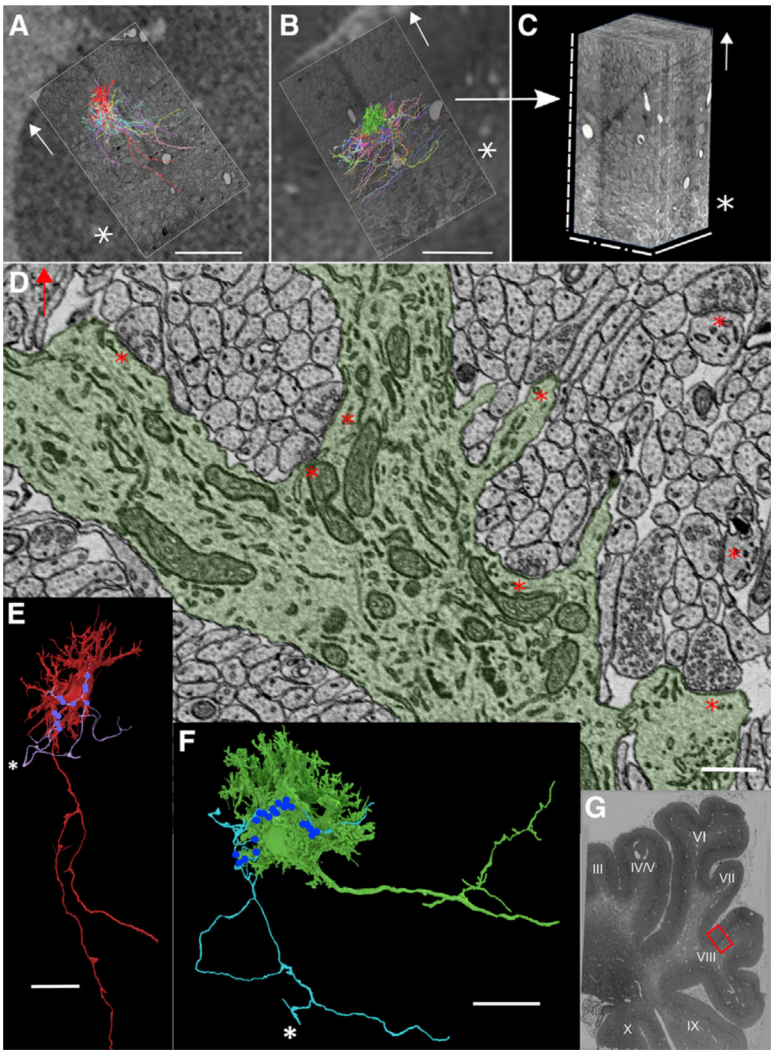

Figure 1. Reconstructions of Climbing Fiber Input to Purkinje Cells in P3 and P7 Mouse Cerebellar Cortex

(A) Low-resolution electron micrograph of tissue used to generate the P3 dataset. The region imaged at high resolution, along with the fully reconstructed Purkinje cell (red) and all its climbing fiber inputs, are superimposed.

(B) Low-resolution electron micrograph of the P7 tissue, shown with a section from the dataset, the fully reconstructed Purkinje cell (green), and all its climbing fiber inputs. Cortical layers for the datasets are shown in Figure S1A; all Purkinje cells are shown in Figures S1B and S1C; closer views of the fully reconstructed cells are shown in Figures S1D and S1E.

(C) The P7 image volume (B). Solid line: through-section axis.

(D) Part of a high-resolution micrograph at P27, showing a dendrite of the fully reconstructed Purkinje cell (green).

(E) Fully reconstructed Purkinje cell at P3 with its most powerful climbing fiber branch input (purple). Dots: synapses formed by this input onto the cell (13 total).

(F) Fully reconstructed Purkinje cell at P7 with its most powerful climbing fiber branch input (blue). Dots: synapses formed by this input (26).

(G) Low-resolution electron micrograph showing cerebellar location of the P7 dataset (red box). The P3 dataset is in the same location.

Arrows: pia (A–D). Asterisks: white matter (A–C); excitatory synapses (D); and volume entry point of climbing fiber branch (E and F). Scale bars: 1100 μm (A and B); 75-μm solid line, 120-μm dot-dashed line, and 190-μm dashed line (C); 0.5 μm (D); 15 μm (E and F); and 190-μm-by-120-μm red box (G).

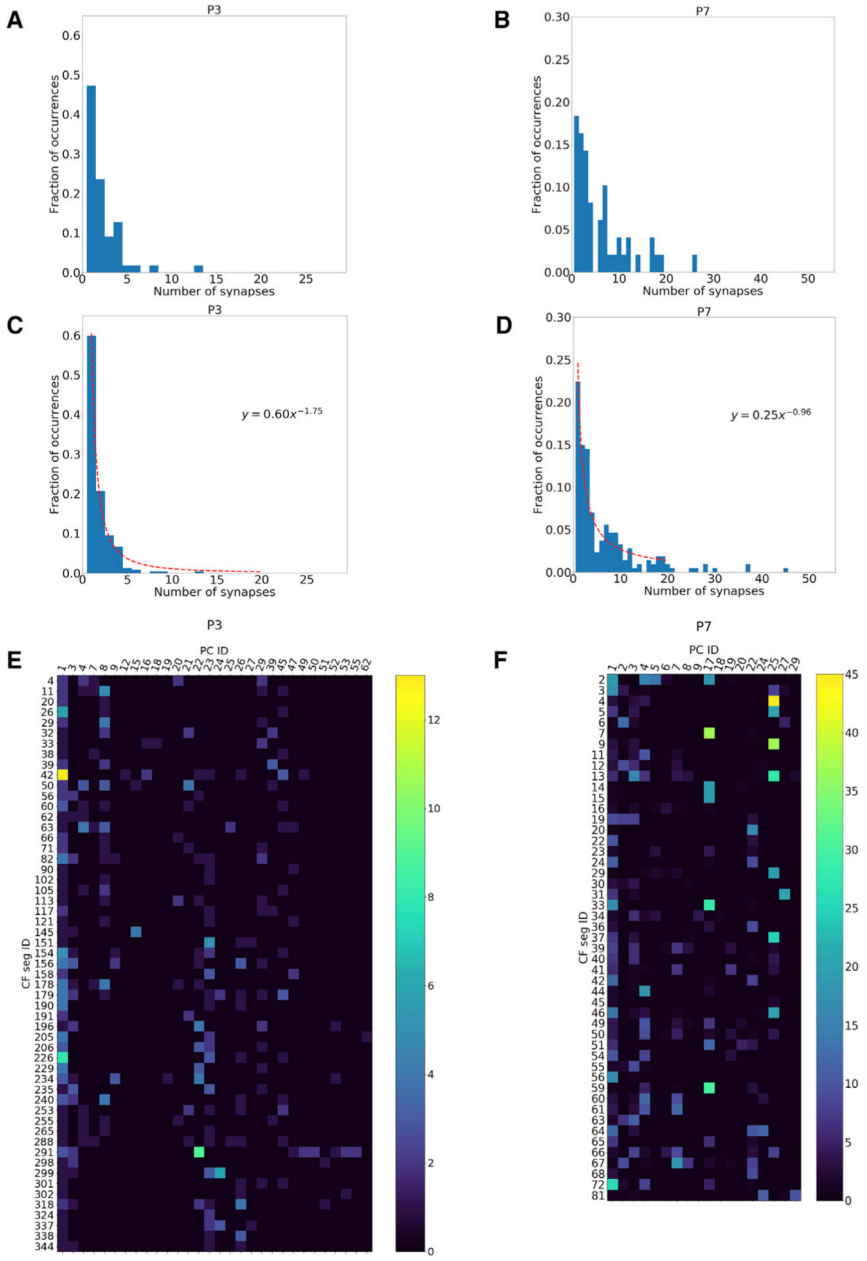

Figure 2. A Small Proportion of Climbing Fiber Branch-Purkinje Cell Connections Consist of Disproportionately Large Numbers of Synapses

(A) Distribution of numbers of synapses formed by climbing fiber inputs (55 branches) to the fully reconstructed Purkinje cell at P3 (127 synapses total). Mean ± SD of this tailed distribution: 2.3 ± 2.1 synapses per connection. Median: 2 synapses per connection.

(B) Numbers of synapses formed by climbing fiber branch inputs (49) to the fully reconstructed Purkinje cell at P7 (298 total). Mean ± SD, median: 6.08 ± 5.7, 4 synapses, respectively.

(C) Numbers of synapses shared by climbing fiber branch-Purkinje cell pairs reconstructed at P3 (242 pairs total, 435 synapses total). Mean ± SD, median: 1.8 ± 1.4, 1 synapse, respectively.

(D) Numbers of synapses shared by climbing fiber branch-Purkinje cell pairs reconstructed at P7 (214, 1,355 synapses total). Mean ± SD, median: 6.3 ± 7.1, 3 synapses, respectively. Monte Carlo simulations (Figure S3) show these distributions are unlikely to result from climbing fiber branches innervating Purkinje cell targets with uniform probability.
(E) Connectivity matrix for reconstructed climbing fiber branches onto Purkinje cell targets at P3. (*i*,*j*)-th element: the number of synapses formed by climbing fiber branch *i* onto Purkinje cell *j*. Climbing fibers and Purkinje cells are identified by segment ID.
(F) Connectivity matrix as in (E) for P7.

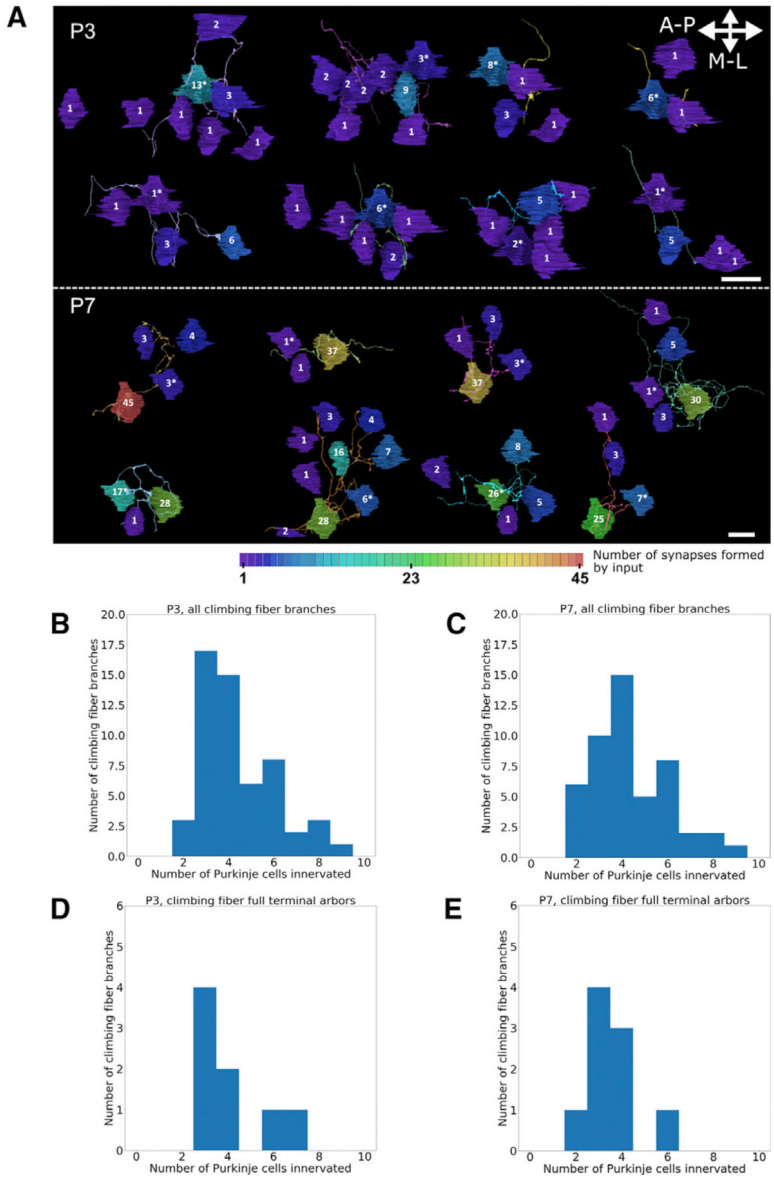

Figure 3. Synaptic Divergence Patterns for Climbing Fiber Branches at P3 and P7

(A) Connectivity onto Purkinje cell targets for the 8 climbing fiber branches forming the most synapses onto single Purkinje cells at P3 (top) and P7 (bottom), viewed dorsoventrally. Target Purkinje cell somas are shown for each branch with the number of synapses formed by that branch (also indicated by cell color, ranging from dark purple at 1 synapse to red at 45). See Figures S4 and S5 and Data S1 and S2. P3 branch IDs, in descending order of maximum number of synapses, are (left to right) 42, 291, 226, 26 (top), 299, 154, 11, and 151 (bottom). P7 branch IDs are 4, 7, 9, 59 (top), 33, 13, 72, and 37 (bottom).

(B) Numbers of Purkinje cells innervated by individual climbing fiber branches reconstructed at P3 (divergence; 55 branches; mean ± SD: 4.4 ± 1.6).

(C) P7 climbing fiber branch divergence (49 branches; mean ± SD: 4.4 ± 1.7).

(D) P3 full terminal arbor divergence (8/55 branches; mean ± SD: 4.1 ± 1.5).

(E) P7 full terminal arbor divergence (9/49 branches; mean ± SD: 3.6 ± 1.6).

Scale bars: 15 μm (A).

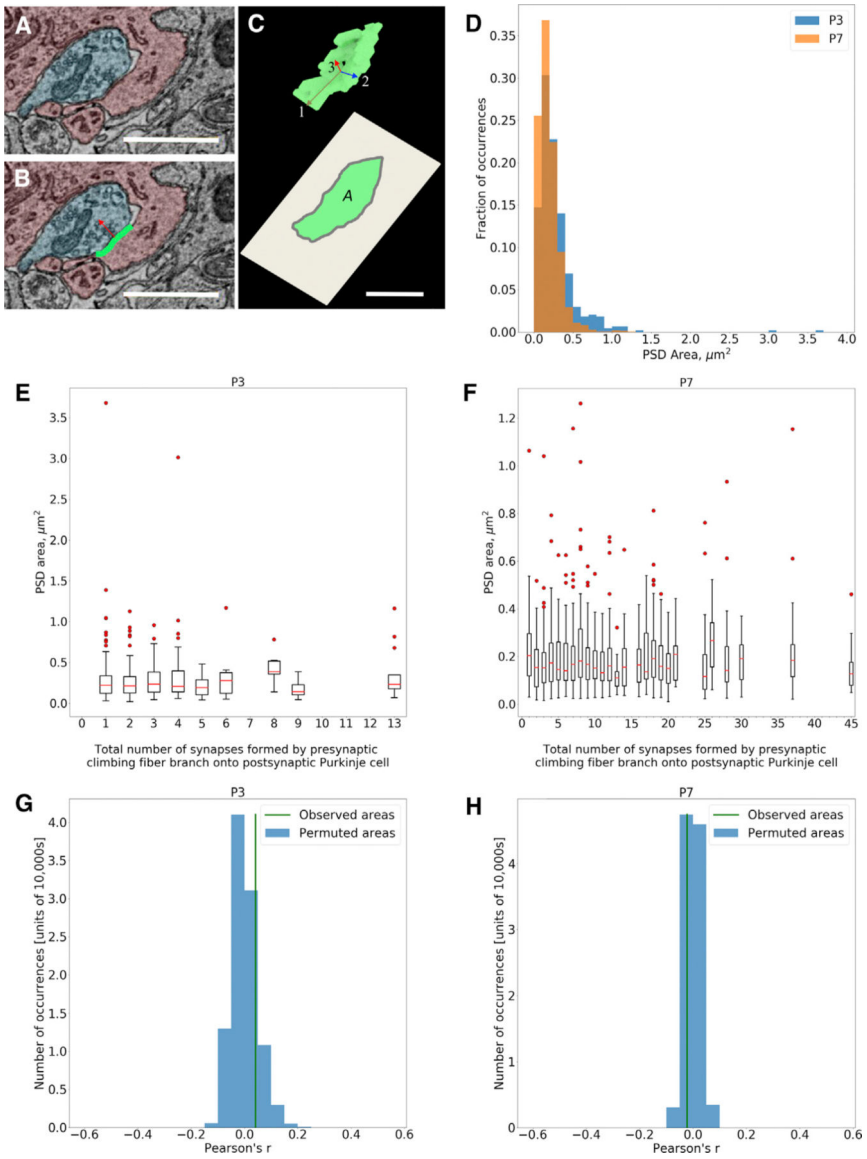

Figure 4. PSD Areas Become More Uniform during the First Postnatal Week and Are Uncorrelated to Climbing Fiber-Purkinje Cell Connection Strength

(A) High-resolution electron micrograph of climbing fiber (blue) to Purkinje cell (red) synapse.

(B) Region in (A) with PSD annotated. Red arrow: normal to the flattest plane of PSD.

(C) Three-dimensional rendering (top) and two-dimensional projection with area A along normal of the flattest plane (bottom) of the PSD in (B). Arrows: principal component vectors of PSD voxel list.

(D) Distributions of PSD areas for all climbing fiber-Purkinje cell synapses identified at P3 (435, blue) and P7 (1,355, orange). $p \sim 0$, Wilcoxon rank sum test.

(E) Boxplot summarizing PSD area of each P3 synapse versus the total number of synapses formed between its presynaptic climbing fiber branch and postsynaptic Purkinje cell.

(F) Boxplot as in (E) for P7 synapses. Boxes (E and F) range from first to third quartiles. Lines denote median. Whiskers denote distances of 1.5 times the interquartile range below first quartile and above third quartile.

(G) Results of a permutation test comparing the observed correlation between PSD area and climbing fiber branch-Purkinje cell connection strength at P3 (green line, from E) against correlations measured when PSD areas are randomly shuffled (blue). $p = 0.38$.

(H) Results of permutation test as in (G) on P7 data (F). $p = 0.41$.

Scale bars: 1 μm (A and B) and 0.25 μm (C).

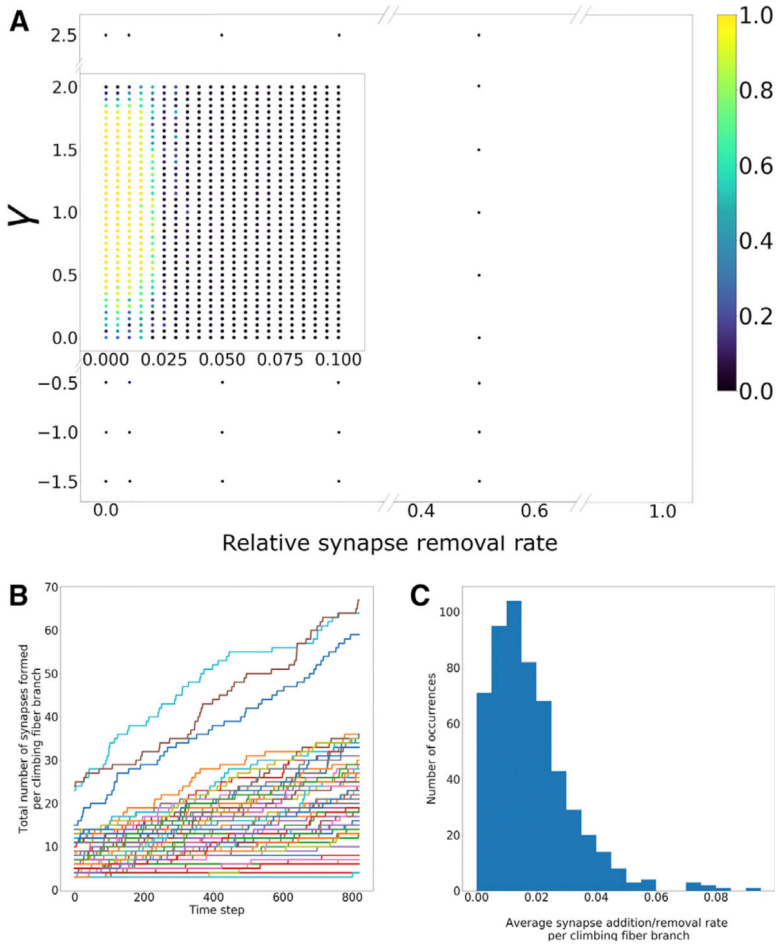

Figure 5. Preferential Addition of Synapses and Minimal Synapse Removal Are Required to Evolve P3 Connectivity to P7 Connectivity

(A) Plot showing the fraction of simulations that successfully evolved observed P3 connectivity into P7-like connectivity, as a function of synapse removal rate and γ. Ten simulations were performed for each parameter value pair. See Figures S6A–S6D.

(B) Total number of synapses formed by each climbing fiber branch at eachtime step of a simulation for a convergent parameter pair (p_{rem} = 0.005, γ = 1.1). Data are shown until the first time step P7-like connectivity was achieved.

(C) Distribution of average synapse addition rates per climbing fiber branch,100 simulations, parameters in (B). Median, maximum: 0.015, 0.092 synapses per time step, respectively.

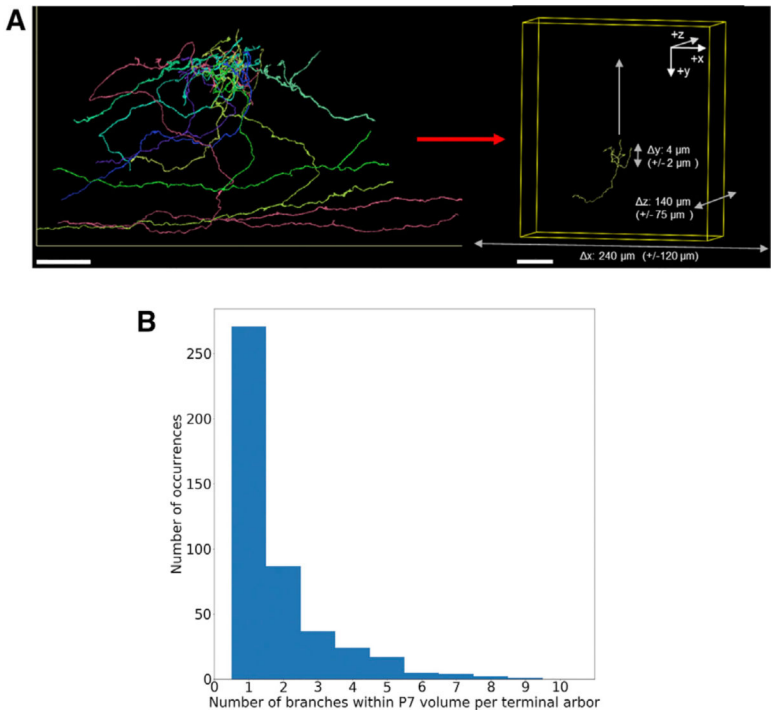

Figure 6. Morphologies of Climbing Fiber Terminal Arbors Allow Estimation of the Number of Branches Produced by Terminal Arbors Split by Image Volume Boundaries

(A) Left: three-dimensional rendering of the 9 reconstructed climbing fiber branches at P7 with full terminal arbors. Right: one branch in the same view, with bounds on random translation used to simulate terminal arbors. Arrow: pia. Z is through-section axis.

(B) Distribution of the number of branches produced by a climbing fiber terminal arbor leaving and re-entering the P7 image volume, 500 simulated terminal arbors. Mean ± SD: 1.8 ± 1.4.

Scale bars in (A): 20 μm (left) and 30 μm (right).

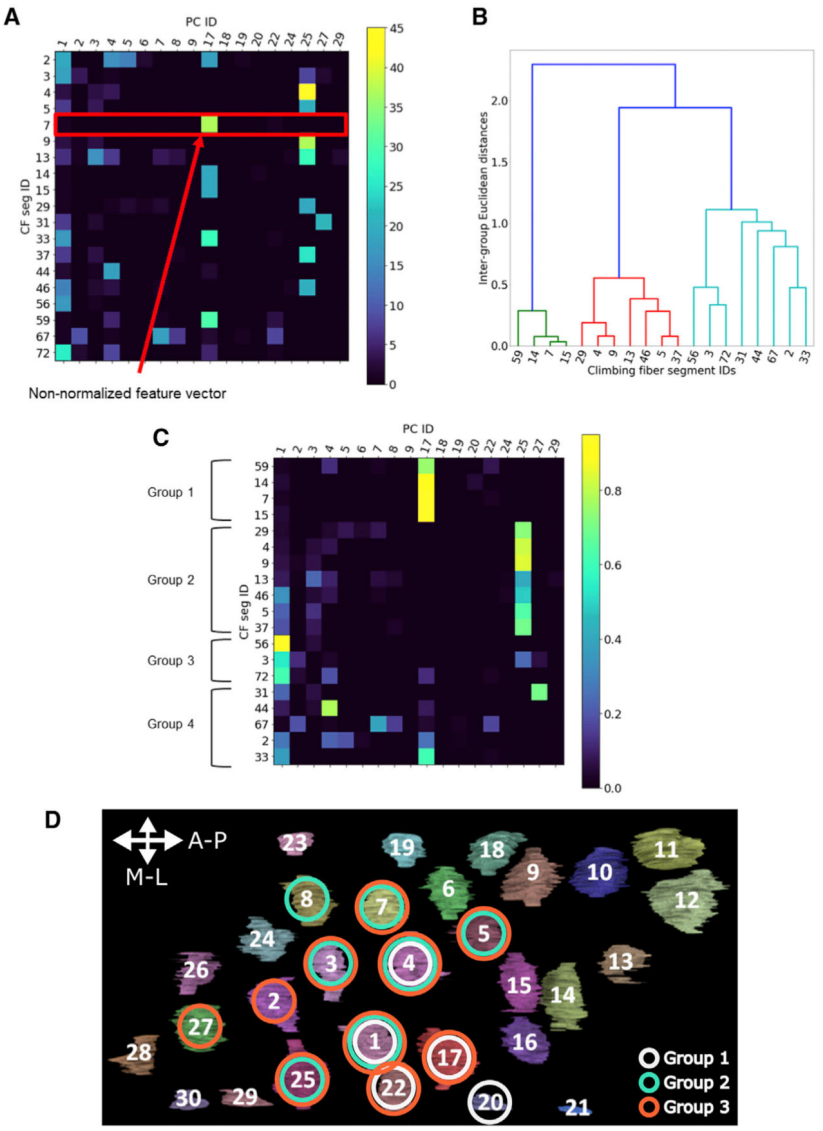

Figure 7. Groups of Climbing Fiber Branches at P7 Have Shared Purkinje Cell Preferences

(A) P7 connectivity matrix for only climbing fiber branches exhibiting strong synaptic preferences. Connectivity for one branch (red box) is a feature vector in Purkinje cell space.

(B) Dendrogram showing hierarchical clustering of P7 branches in (A).

(C) Normalized P7 connectivity matrix, reordered following (B). Groups 1–3 each contain branches that share rankings of preferred Purkinje cells. Group 4 contains branches with Purkinje cell rankings that differ from those of groups 1–3 and other branches in group 4.

(D) Preferred Purkinje cells for groups with shared preferences from (C), viewed dorsoventrally. Gray, cyan, and orange circles: cells preferred by groups 1, 2, and 3, respectively. Purkinje cells are labeled by segment ID. Scale bar: 15-micron anteroposterior axis marker.

KEY RESOURCES TABLE

REAGENT or RESOURCE	SOURCE	IDENTIFIER
Chemicals, Peptides, and Recombinant Proteins		
Paraformaldehyde, 16% aqueous solution	Electron Microscopy Sciences	Cat#15710, CAS: 30525–89–4
Glutaraldehyde, 25% aqueous solution	Electron Microscopy Sciences	Cat#16220, CAS: 111–30–8
Osmium tetroxide, 4% aqueous solution	Electron Microscopy Sciences	Cat#19190, CAS: 20816–12–0
Potassium ferrocyanide	Sigma Aldrich	60279, CAS: 14459–95–1
Thiocarbohydrazide	Sigma Aldrich	223220, CAS: 2231–57–4
Epon 812 resin	Electron Microscopy Sciences	Cat#14120
Uranyl acetate	Electron Microscopy Sciences	Cat#22400, CAS: 541–09–3
Lead citrate	Leica	Leica Ultrostain II, CAS: 6107–83–1
Deposited Data		
Electron microscopy image volumes and annotations	This paper; Johns Hopkins University Applied Physics Laboratory's BOSS	https://bossdb.org/project/wilson2019
Raw data	This paper; Mendeley	https://doi.org/10.17632/jsjny43yzz.1
Experimental Models: Organisms/Strains		
Mouse: Timed Pregnant CD-1	Charles River	N/A
Software and Algorithms		
WaferMapper	Hayworth et al., 2014	N/A
VAST Lite	Berger et al., 2018	https://software.rc.fas.harvard.edu/lichtman/vast/
Mojo	Knowles-Barley et al., 2013	N/A
Kimimaro	Github	https://github.com/seung-lab/kimimaro
Igneous	Github	https://github.com/seung-lab/igneous
Analysis scripts	This paper; Github	https://github.com/amwilson149/baby-andross